2012

A performance comparison between water and IAS-charged thermosyphons

Stephen D. Cooke

A PERFORMANCE COMPARISON BETWEEN WATER AND IAS-CHARGED THERMOSYPHONS

by

STEPHEN D. COOKE

A THESIS

Submitted in partial fulfillment of the requirements
for the degree of Master of Science in Engineering
in
The Department of Mechanical and Aerospace Engineering
to
The School of Graduate Studies
of
The University of Alabama in Huntsville

HUNTSVILLE, ALABAMA

2012

In presenting this thesis in partial fulfillment of the requirements for a master's degree from The University of Alabama in Huntsville, I agree that the Library of this University shall make it freely available for inspection. I further agree that permission for extensive copying for scholarly purposes may be granted by my advisor or, in his/her absence, by the Chair of the Department or the Dean of the School of Graduate Studies. It is also understood that due recognition shall be given to me and to The University of Alabama in Huntsville in any scholarly use which may be made of any material in this thesis.

Stephen D Cooke
(student signature)

03-12-12
(date)

THESIS APPROVAL FORM

Submitted by Stephen Cooke in partial fulfillment of the requirements for the degree of Master of Science in Mechanical Engineering and accepted on behalf of the Faculty of the School of Graduate Studies by the thesis committee.

We, the undersigned members of the Graduate Faculty of The University of Alabama in Huntsville, certify that we have advised and/or supervised the candidate on the work described in this thesis. We further certify that we have reviewed the thesis manuscript and approve it in partial fulfillment of the requirements for the degree of Master of Science in Mechanical Engineering.

3/12/12 _____ Committee Chair
(Date)

3/12/2012 _____

3/12/2012 _____

_____

_____ Department Chair

_____ College Dean

Rhonda Kay Gaede 3/27/12 Graduate Dean

ABSTRACT
The School of Graduate Studies
The University of Alabama in Huntsville

Degree Master of Science in Engineering College/Dept. Engineering/Mechanical and Aerospace Engineering

Name of Candidate Stephen David Cooke

Title A Performance Comparison Between Water and IAS-Charged Thermosyphons

An inorganic aqueous solution (IAS) has recently become a topic of interest among thermal engineers. The fluid has been used to reportedly charge so-called "Qu tubes", and has demonstrated high heat transport capability in capillary wicks in comparison to water. It has also shown promise as an aluminum compatible aqueous solution. This study measures the axial heat flux of 10 ft. long, 5/16 in. diameter water and IAS-charged thermosyphons in a forced convection apparatus at heater inputs of 300W, 450W, 600W, and 700W. The performance of the thermosyphons was measured at angles of 35, 25, and 15 degrees from horizontal for power levels up to 600W. The performance was measured at an angle of 35 degrees from horizontal for a heater input of 700W. An air calorimeter was used to quantify the condenser-end heat rate of the tubes. The performance was also measured with the heater temperature in conjunction with a power-loss curve that was determined by experiment. The water and IAS-filled tubes displayed equivalent performance up to a supplied power of 450W. The IAS-filled tube showed signs of dryout at 600W, while the water-filled tube achieved steady-state operation up to a heater input of 700W. An overall axial heat flux of 1276.5 W/cm^2 was obtained for a heater input of 700W for the water thermosyphon. Internal axial grooves internal to the water-filled tube may have

contributed to its performance at higher temperatures. The axial heat fluxes for both tubes fall well below analytical predictions of numerous closed-form thermosyphon limiting equations.

Abstract Approval

Committee Chair

Department Chair

Graduate Dean Rhonda Kay Faede 3/27/12

ACKNOWLEDGEMENTS

Thank you to my wife, Janelle, for your constant love, understanding, and support. Thank you also to my sons, Caleb and Samuel, for being such great boys.

Thank you to my committee members, Dr. Blackmon, Dr. Wessling, and Dr. Cassibry, for serving on my committee and offering meaningful help and advice when needed. Dr. Blackmon provided a good deal of guidance, and was instrumental in channeling ASI's Phase I SBIR into something that could be extended into a thesis effort.

Thank you to my boss, Dr. Joe Sims, who has been extremely understanding and flexible while I have worked toward an advanced degree.

Thank you to my parents for raising me right, and to my sister, Holly, who is a quiet inspiration.

I am thankful to God for every opportunity granted in life, and for the joy in which I can live through the forgiveness of sins.

This material is based upon work supported by the Air Force Research Laboratory under Contract No. FA9453-10-M-0143

TABLE OF CONTENTS

LIST OF FIGURES

Figure **Page**

LIST OF TABLES

Table **Page**

LIST OF SYMBOLS

A	cross-sectional area, m^2
A_v	area of thermosyphon vapor space, m^2
Bo	Bond number, $D\left[g\left(\frac{\rho_l - \rho_v}{\sigma}\right)\right]^{1/2}$
C_p	specific heat, J/(kg-K)
C_w	empirical constant, Wallis correlation
D	pipe diameter, m
D_c	diameter of the condenser section, m
D_e	diameter of the evaporator section, m
g	gravitational constant, m/s^2
h_f	natural convection film coefficient, $W/(m^2\text{-}K)$
h_{fg}	latent heat of vaporization, J/kg
L	length, m
L_{ac}	length of the adiabatic section having the same diameter of the condenser section, m
L_{ae}	length of the adiabatic section having the same diameter of the evaporator section, m
L_e	length of the evaporator section, m
Nu_d	diameter dependent Nusselt number
Nu_L	length dependent Nusselt number
$Nu_{L,ave}$	average length dependent Nusselt number for a heated surface

Pr	Prandtl number
Q	heat rate, W
$Q_{condenser}$	rate of heat loss in the condenser section, W
q_{crit}	critical radial heat flux at the evaporator, W/m^2
$Q_{in`}$	input power, W
$Q_{loss\_adiabatic}$	rate of heat loss in the adiabatic section, W
Q_{loss_heater}	rate of heat loss in the heater section, W
Q_{tube}	heat rate transported by the tube, W
R	radius, m
Ra_D	diameter dependent Rayleigh number, $\beta \Delta T g D^3 Pr/v^2$
Ra_L	length dependent Rayleigh number, $\beta \Delta T g L^3 Pr/v^2$
T_{in}	average temperature at the calorimeter inlet, K
T_{out}	average temperature at the calorimeter outlet, K
U_x	95% uncertainty interval corresponding to a variable 'x'
V'	fill volume ratio (V_l / V_e)
V^+	fill volume (V_l / V_t)
V_e	volume of the evaporator section, m^3
V_{exit}	air velocity at the calorimeter exit, m/s
V_l	liquid volume, m^3
V_t	total fill volume, m^3
W	width of thermosyphon axial grooves, m

GREEK SYMBOLS

β	inverse of the reference temperature, K^{-1}
μ	dynamic viscosity, kg/(m-s)
ν	kinematic viscosity, m^2/s
ρ_l	liquid density, kg/m^3
ρ_v	vapor density, kg/m^3
σ	surface tension, N/m
Ψ	Prandtl number function

CHAPTER ONE

INTRODUCTION

An inorganic aqueous solution (IAS) has recently become a topic of interest among thermal engineers as a potential replacement for water in heat pipes and thermosyphons. The water-based fluid contains a low concentration of chemical additives, the majority of which are chromate and dichromate salts [9]. The fluid has become recognized as a likely heat flux performance enhancer in capillary wicking structures in comparison to water, and has also shown promise as an aluminum-compatible solution [1], [9]. The latter quality has especially captured the attention of thermal engineers that are pressed by low weight design requirements. Since water itself is not compatible with aluminum and aluminum alloys, an IAS-charged heat pipe or thermosyphon offers the potential to improve substantially upon the current state-of-the-art in these technologies on a heat-rate per unit-mass basis. This is because water is most generally used in combination with higher density materials like copper or monel. Indeed, water is sometimes used in lower weight titanium heat pipes, but the lower thermal conductivity of the metal and its extremely high costs hardly make it worthwhile [17]. Setting the potential of aluminum-IAS compatibility aside, there is still an interest to gauge the overall heat transfer capability of IAS relative to water in heat pipe applications [9].

Although IAS has just recently been thrust into the spotlight as a potentially novel heat pipe working fluid, there is actually plenty of performance data for IAS-charged heat pipes and thermosyphons that is publicly available. This is because the solution was used to charge pipes that have been previously classified as “Qu tubes” [9], which have been subjected to numerous performance evaluations in studies dating back to 1999. Notable organizations that have characterized various (dimensionally different) forms of the tube include Stanford Research Institute International (SRI International) [12], the Air Force Research Laboratory (AFRL) [13], the National Aeronautics and Space Administration (NASA) [14], and the

University of Alabama in Huntsville (UAHuntsville) [15], [16]. The aforementioned studies were precursors that eventually led to the realization that "Qu tubes" were IAS-charged heat pipes and thermosyphons, rather than solid state heat transfer devices as had been claimed previously [18]-[21]. As mentioned earlier, more recent studies have focused specifically on the IAS working fluid and its favorable properties. The entire culmination of studies represent a kind of "Qu tube" to IAS transition as far as the overall experimental focus is concerned. Of course, the more recent focus on IAS is the result of a better understanding of the internal operation of the tubes in general. The studies are each summarized below as they contribute to the history of IAS, and demonstrate a slow progression to its recognition as a potentially notable working fluid for passive, two phase heat transfer devices.

1.1 Previous "Qu tube" and IAS-Related Studies

Early "Qu tube" related studies seemed to generate "inconclusive and mixed opinions" [13] among thermal scientists in the short time after the tubes were first patented in the year 2000. The original patent claimed that the tubes contained a solid-state, superconducting heat transfer medium that was formed by evaporating three distinct chemical mixtures in sequence out of the bore of the tube. The result was the formation of three sequential chemical layers that were deposited on the tube wall. These are aptly described by Rao in his 2009 thesis [16]. The prescribed process for mixing each of the various chemical solutions is murky at best, as the exact concentration of each of the specific chemical additives is never stated explicitly [18]. The patent also contains other questionable nuances like warnings of catastrophic reactions if chemical additives were added to their respective solutions in the wrong order, and a description of a blue light that could possibly emerge from the tube bore during the evaporation process. Four patents in total were awarded to the inventor, Yuzhi Qu. The second patent, awarded in 2004, consolidates the three chemical layers into a single one in order to (according to the patent) reduce the number of compounds and steps needed to produce a superconducting chemical wall layer [19]. The third patent, awarded in 2005, laid claim specifically to the *method* for producing the superconducting wall layers that were described in the first patent [20]. The fourth, also awarded in 2005, seems to build on the first and third patents by simply adding a few additional claims regarding chemical preparation and

purity levels [21]. Overall, the patents claimed that the tubes could (as adequately summarized in [13]): operate with no liquid in the tube (solid state heat transfer), transfer heat without any net temperature gradient, be made in nearly any geometry, and be fabricated using a wide range of metals.

At the time, the extraordinary claims of the patents might have generated enough pessimism among heat pipe enthusiasts for the idea of a solid state heat pipe to be disregarded altogether. However, their performance was allegedly confirmed by sound independent tests. This is where the work done by SRI International enters the picture, as they conducted the earliest known studies on the "Qu tubes" which were later used to substantiate the claims of the patents.

The studies conducted by SRI International actually pre-date the first "Qu-tube" patent that was granted in 2000. The studies characterized the tube performance by observing temperature transients in a natural convection set-up. The performance was also quantified using a water calorimeter. The tubes tested were 2.5cm in diameter and 1.2m long. Among the findings was an "anomalous" sinusoidal temperature distribution where the temperature of the heated end of the tube was less than the end opposite the heater. Those observations were made during a single natural convection transient period where the temperature along the length of the tube was recorded over time while the heater power was increased from 10 W to 178 W [11]. The tube was also reported to have high transport efficiencies in the calorimeter setting where an axial heat flux of 2.5×10^6 W/m^2 (250 W/cm^2) was observed [12]. Also, by analysis, the tube was found to have an effective thermal conductivity of 1000 times that of silver [11]. Finally, SRI International conducted a number of animal studies with mice and rabbits to determine the oral limit, as well as the eye and dermal irritation effects of the "Qu tube" powder [15]. The studies in their entirety were used to promote the (alleged) exceptional heat transfer performance of the "Qu tube", and non-hazardous qualities of the superconducting medium on the pipe wall [15]. Indeed, the calorimeter study conducted by SRI International is quoted verbatim in Qu's 2004 patent [19]. At the date of this publication, those reports are publicly available through the website of a Hong Kong based company, Quantum Technology Group [23].

In 2003, scientists at NASA Langley Research Center (LaRC) entertained the possibility of using "Qu tubes" for a fuel cell heat exchanger that was part of a conceptual design for an emissionless aircraft

[14]. In that report, a number a demonstrations are cited that supported claims of high effective thermal conductivity through the tube. The "Qu tubes" were considered specifically for the potential in heat exchanger weight savings that could be attributed to their innate solid state operating characteristics and the fact that the chemical coating was reportedly (according to Dr. Qu's engineers) compatible with aluminum pipes. The report was exploratory in nature and was meant to summarize technologies that could potentially make the idea of an emissionless aircraft feasible.

In 2010, the AFRL released a report that summarized a "Qu tube" related study that dates back to 2004 [13]. In that effort, the performance of a 0.750 in. diameter, 28 in. long steel tube was quantified using a water calorimeter. Temperature gradients along the length of the tube were measured with thermocouples calibrated against an ice point to an accuracy of $\pm$ 0.1^{o}C. Overall, the maximum effective thermal conductivity was found to be 15,000 W/mK, much lower than that reported by the "Qu tube" patents. The tube was reportedly tested at input power levels up to 350 Watts. The calorimeter only absorbed about 20% of that power, which indicated substantial heat loss along the length of the tube. Assuming that all of the power supplied by the heater had entered the tube in the evaporator section, the tube would have demonstrated a maximum operating heat flux of about 140 W/cm^{2}. In addition, the tube only showed the ability to reach steady-state operating temperature in a gravity assisted position (when the evaporator was lower than the condenser). Upon cutting open the tube, scientists found approximately 10mL of water. A spectral analysis showed that the liquid residue had contained trace amounts of what was deduced to be potassium dichromate. The conclusion was that the tube offered no real breakthrough with regard to current state-of-the-art heat transfer technologies. However, it was also noted that the tubes obtained by the AFRL were not explicitly validated by the inventor as "Qu tubes".

In 2006, reports were published by researchers at UAHuntsville to summarize some exploratory investigations of the tubes that had been funded through NASA's Technology Maturation Program (TMP) [4], [22]. Tubes that were 5/16 in. in diameter by 17 in. and 10 ft. long were tested in an attempt to quantify the effective thermal conductivity of the tube. The exposed end of the 17 in. long tube was lined with four thermocouples (with an accuracy of $\pm$ 2.2^{o}C) along its length, and oriented vertically in a beaker of boiling water. Using the observed axial temperature gradients along the tube in conjunction with a

billet analysis of an annular copper rod, the effective thermal conductivity was found to be 10,000 times that of copper. A 10 ft. long tube was similarly lined with thermocouples and tested at an incline in a natural convection set-up. The effective thermal conductivity of the longer tube was found to be approximately 30,000 times that of copper by the same method of analysis. The tubes were also subjected to gravity-dependent tests in which only some of the tubes were able to operate against gravity. Finally, an X-ray of the tubes revealed a circumferential wire mesh spanning the length of the tube that was in contact with the inner pipe wall.

UAHuntsville's exploratory investigation for NASA laid the groundwork for more rigorous studies that would be conducted by that institution. The first was a study conducted by Entrekin, published in 2008 [15], specifically designed to precisely measure the thermal gradients along the length of a 5/16 in. diameter, 10 in. long tube that was cooled by a water calorimeter. The tube's small diameter could easily facilitate large axial heat flux values (W/cm^2) with minimal power input. In addition, the combination of long length and small diameter would have made it impossible for the tubes to operate against gravity by means of an internal capillary wick. This meant that any high performance observed in a gravity independent orientation would have been necessarily due to unique operating characteristics intrinsic to the tube itself. Twenty-four calibrated thermistors ($\pm$ 0.1^{o}C) spread equidistantly over a 100 cm span in the adiabatic section were used to measure axial temperature gradients along the length of the tube. A detailed uncertainty analysis showed the temperature gradient measurements had an experimental uncertainty of $\pm$ 0.14^{o}C. An intricate thermistor rake was also used to minimize installation errors, ensuring that each of the thermistors had good contact with the tube wall. The tube showed nearly constant temperatures along its length, with no observable sinusoidal temperature variations like those reported by SRI International. The tube was indeed gravity dependent, operating as a normal, uncharged copper tube with the condenser below the evaporator. Maximum heat flux values obtained in the study were on the order of 650 W/cm^2.

An additional study conducted at UAHuntsville in 2009 by Rao essentially explored the maximum heat flux that could be attained through the tube in a forced convection setting [16]. Since the performance of the tube could not be measured directly by means of a calorimeter, UAHuntsville

researchers developed a unique method to estimate the amount of power lost through the heater insulation. In effect, the method allowed researchers to measure the axial heat fluxes that were being supported by the tube. This was done by removing the tube from the heater assembly and recording the heater temperature at various power input levels. In this configuration, the heat supplied to the heater was assumed to be equal to the heat lost through the surrounding insulation. A power-loss curve was then developed to determine the heat lost through the heater insulation as function of heater temperature. Rao was able to obtain an axial heat flux of 1,043 W/cm^2 in his study. He also reported the observation of a possible radial limitation to heat flux into the tube, which could not be fully investigated.

The studies conducted by UAHuntsville raised serious question regarding the "Qu tube's" purported solid state operating characteristics. Although the effective thermal conductivity of the 10 ft. long tube was indeed high, as were the attained axial heat fluxes, the tubes still exhibited a gravity dependence that was similar to what would be expected for a thermosyphon. In fact, the UAHuntsville studies had initiated some correspondence among experts in the thermal community with regard to that very thought. The Los Alamos National Laboratory conducted an analysis for UAHuntsville and UCLA researchers in 2010 to determine the limiting heat transfer rates for a water thermosyphon of the same dimensions as the tubes tested at UAH [10]. This was done using a variety of closed-form thermosyphon limiting equations. Their analysis showed that the heat fluxes observed in Entreken's study were completely within the operating realm of an equivalent water-filled thermosyphon. A similar independent analysis was completed for scientists at UAHuntsville by researchers at Trinity College in Dublin, Ireland [8]. These were consistent with the Los Alamos analysis, stating that a conservative value for the limiting heat flux was approximately 1200 W/cm^2. This, of course, was somewhat higher than the axial heat flux attained by Rao, which was the highest that had been published to date at that time.

A more recent study conducted jointly between a Huntsville-based defense contractor, Analytical Services, Inc., and UAHuntsville performed an experimental comparison between a water-charged thermosyphon and a "Qu-tube", which later became more accurately recognized during the course of that study as an IAS-charged thermosyphon. The study was performed under a Phase I SBIR contract awarded by the AFRL [1]. The SBIR solicitation requested the development of a high temperature heat pipe with

the capability of operating in the temperature range of 100 to 200^{o}C, and the ability to survive a freeze-thaw cycle with temperatures as low as -60^{o}C. At the time, the then-called "Qu tube" was proposed for the effort, since it had shown potential for high performance at high operational temperatures in the previous UAHuntsville studies [15], [16].

Prior to the AFRL SBIR, UAHuntsville had obtained three 10 ft. long, 5/16 in. diameter internally grooved "Qu tubes" along with an equivalent water-charged thermosyphon. During the course of that SBIR effort, it became apparent through discussions with the "Qu tube" supplier that the tubes were charged with the aforementioned IAS working fluid (an MSDS is supplied in the Appendix). Consequently, in addition to conducting the tasks intrinsic to the SBIR, a performance comparison was conducted between the water and IAS-filled tubes. Both were tested at an incline of 35 degrees from horizontal at heater inputs to the evaporator ranging from 300 to 750 Watts. The condenser-end heat rate was quantified using an air calorimeter. Overall, the measured performance of both tubes was nearly equivalent, with the water-filled thermosyphon outperforming the IAS-filled thermosyphon outside the bounds of uncertainty at higher operational power levels. The performance difference was approximately 9% for a heater input value of 750 Watts. The uncertainty associated with the calorimeter was estimated to be approximately $\pm$ 30 Watts (4% of the maximum heater input value).

Comparative studies to determine the performance difference between the water and IAS working fluids have also been conducted at UCLA [9]. The referenced study was carried out using a copper biporous evaporator. The results showed that the IAS working fluid outperformed water initially; however, the deposits on the biporous wick caused a decrease in the evaporator performance over time. Those deposits were thought to be due to the chromates coming out of solution, or a chemical reaction with the copper [9]. In that same study, UCLA has also reported an ongoing compatibility test using IAS in aluminum heat pipes. The heat pipes were reported to run for a series of months without failure or signs of production of any noncondensible gases (NCGs).

Finally, UCLA researchers have cited studies conducted at Trinity College in which the IAS was found to outperform water in equivalent, relatively small thermosyphons [3]. The thermosyphons tested were 9mm in diameter and 90cm in length. The tubes were heated from the bottom and cooled by

natural convection in a vertical orientation. In those studies, the thermal resistance of the IAS-filled thermosyphon was reported to be less than half of that of the water thermosyphon. Additionally, the water thermosyphon reportedly reached a dryout condition in the evaporator at lower power levels than the IAS-filled tube.

1.2 Research Objectives

The objective of this study is to expand on the results found in the joint study conducted by ASI and UAHuntsville. The desire is to confirm the relative performance difference observed in that study between the water and IAS-filled thermosyphons using an improved measurement technique that is able to quantify the tube heat rates with a lower amount of inherent uncertainty. Specifically, it is desired to find the heat rate dissipated through the heater insulation as a function of heater temperature, as was first done by Entrekin [15] and later by Rao [16]. The tube heat flux can then be quantified by measuring the temperature of the heater during steady state operation. The heat rate will also be measured in the condenser section using an air calorimeter, as in the ASI/UAHuntville effort.

An additional objective is to measure the performance of the tube at different angular orientations, using an A-frame set-up that was also used in previous UAHuntsville studies, and in the joint ASI/UAHuntsville effort under the AFRL SBIR. Also, the previous studies at UAHuntsville were able to obtain an axial heat flux of 1,043 W/cm^2 where the tubes tested did not have internal grooves [16]. In this study it is desired to determine if a higher axial heat flux can be attained using the internally grooved thermosyphons that were used in [1] (a final report written by ASI which summarizes the work done under the AFRL SBIR). Finally, it is desired to compare the axial heat flux measurements for both tubes against theoretical performance estimates that are generated by using thermosyphon limiting equations.

1.3 Thermosyphon Limiting Equations

A wide range of equations have been developed to predict the heat rate limitations in thermosyphons for different modes of operational failure. Faghri has listed a number of limiting equations in his text [3]. Many of those are summarized below, and are used to predict the theoretical performance of the thermosyphons tested in this study.

The flooding limit is described as a major limiting factor in thermosyphon operation and occurs when high axial heat fluxes are being carried by the tube. Large velocities in the vapor core cause large interfacial shear stresses in the surface of the fluid moving down the pipe wall. With the shear forces, the condensate on the pipe gets held up in the condenser section of the pipe, thereby drying out the evaporator. The flooding limit, then, describes the heat rate at which flooding occurs in the condenser section of the thermosyphon.

The Wallis correlation is reportedly based on water-gas experiments in an open channel. That correlation, dating back to 1969 [25], is described below:

$$\frac{Q}{A} = \frac{Cw2\, h_{fg} \sqrt{g\, D\, (\rho_l - \rho_v)\rho_v}}{[1 + (\rho_l/\rho_v)^{\frac{1}{4}}]^2} \tag{1.1}$$

Where Q is the heat rate, A is the cross-sectional area, h_{fg} is the latent heat of vaporization, g is the gravitational constant, ρ_l is the density of the liquid, ρ_v is the density of the vapor, D is the diameter of the pipe, and C_w is an empirical constant. Faghri points out that C_w values from 0.7 to 1.0 are most commonly reported in the literature [3].

Another equation to predict the flooding limit in thermosyphons was derived by Faghri in 1989 [26]. The equation takes into account the surface tension of the fluid and is considered the most general equation in existence for predicting the limiting heat rate in thermosyphons [3]. That equation is detailed below:

$$\mathrm{Q_{max}} = K\, h_{fg}\, A\, [g\, \sigma\, (\rho_l - \rho_v)]^{1/4} \left[\rho_v{}^{-1/4} + \rho_l{}^{-1/4}\right]^{-2} \tag{1.2}$$

$$\mathrm{K} = \left(\frac{\rho_l}{\rho_v}\right)^{0.14} \tanh^2 \mathrm{Bo}^{1/4} \tag{1.3}$$

$$\mathrm{Bo} = \mathrm{D} \left[\mathrm{g} \left(\frac{\rho_l - \rho_v}{\sigma}\right)\right]^{1/2} \tag{1.4}$$

where σ is the surface tension of the fluid and Bo is the Bond number.

The dryout limitation occurs when a thermosyphon is charged with an inadequate fill volume. The fluid circulates within the thermosyphon, but the film thickness along the inner wall approaches zero at the evaporator end. This corresponds to an evaporator dryout at high heat fluxes. The equation below is apparently an improved model based on an equation derived by Shiraishi in 1984 [27]. It was found to correspond well with experimental data for fill ratios (defined below) between 0.10 and 0.20. The dryout equation is as follows:

$$\left(\frac{Q_{crit}}{\rho_v\, h_{fg}}\right)\left[\frac{g\,\sigma\,(\rho_l-\rho_v)}{{\rho_v}^2}\right]^{-\frac{1}{4}} = \left[\frac{g\,{\rho_l}^2\left(\frac{D_c}{D_e}\right)}{3\,\mu\,L_e\sqrt[4]{\sigma\; g\,{\rho_v}^2\,(\rho_l-\rho_v)}}\right]\left[\frac{\frac{V_t}{(\pi\,D_c)}}{\frac{4\,L_c}{5}+L_{ac}+\left(\frac{D_e}{D_c}\right)^{\frac{2}{3}}\left(L_{ae}+\frac{3Le}{4}\right)}\right]^3\left[\frac{(V_e/V_t)(V')-\rho_v/\rho_l}{1-\rho_v/\rho_l}\right]^3 \quad (1.5)$$

where q_{crit} is the critical radial heat flux at the evaporator, μ is the dynamic viscosity of the liquid, D_c is the diameter of the condenser section, D_e is the diameter of the evaporator section, L_e is the length of the evaporator section, L_{ae} is the length of the adiabatic section that has the same diameter as the evaporator section, L_{ac} is the length of the adiabatic section that has the same diameter as the condenser section, V_t is the total fill volume, V_e is the total volume of the evaporator section, and V' is the fill volume ratio defined as (V_l / V_e), where V_l is the volume of the liquid in the thermosyphon. Since the thermosyphons tested in this study had a constant diameter along the length of the tube, L_{ae} was taken to be equal to L_{ac}, both values being half the length of the adiabatic section. Going along with the same line of thought, D_c was set equal to D_e. The effect of the adiabatic length assumption was tested by finding the value of q_{crit} assuming L_{ae} = 1 and L_{ac} = 0, and then inversely assuming L_{ae} = 0 and L_{ac} = 1. The results showed that varying the respective lengths of the adiabatic section had a minute effect on the value of q_{crit}, as long as the diameter was the same throughout the length of the pipe (D_c = D_e).

The boiling limitation occurs in pipes capable of supporting large internal fill volumes. When high heat rates are applied to the evaporator section, nucleate boiling begins to occur. As heat rates are

increased, the boiling phenomenon eventually separates the working fluid from the pipe wall altogether. Since the thin vapor film has a much high thermal resistance, this corresponds to a boiling heat transfer "burn out" condition. The wall temperatures then rise substantially and the thermosyphon has an increased chance of rupture. Faghri summarizes a boiling limitation developed by Gorbis and Savchenkov that was developed in 1976 [28]. That equation is as follows:

$$\frac{q_{max}}{q_{max,\infty}} = C^2 h_{fg}\left[0.4 + 0.12R\sqrt{\frac{g\,(\rho_l-\rho_v)}{\sigma}}\right]^2 \tag{1.6}$$

$$q_{max,\infty} = 0.142\sqrt{\rho_v}\,[g\,\sigma\,(\rho_l - \rho_v)]^{1/4} \tag{1.7}$$

$$C = A\left(\frac{D}{L_c}\right)^{-0.44}\left(\frac{D}{L_e}\right)^{0.55} V^{+n} \tag{1.8}$$

$$A = 0.538, n = 0.13 \quad for \quad V^+ \leq 0.35$$

$$A = 3{,}53, n = -0.37 \quad for \quad V^+ > 0.35$$

where R is the radius of the thermosyphon, and V^+ is the fill volume defined as (V_l / V_t). The equation is applicable for tilt angles ranging from 0° to 86° from vertical, and for fill volumes in the range of 0.029 to 0.60.

Finally, Faghri also provides an equation for the entrainment limit for thermosyphons with grooved wicks. The correlation was developed through the efforts of Tien in 1977 [29], and Tien and Chung in 1978 [30]. The entrainment limit is described by the following equation:

$$Q = 3.2\sqrt{\frac{D}{W}}\left[\tanh\left(0.5Bo^{1/4}\right)\right]^2 A_v\, h_{fg}\left[\rho_v{}^{-1/4} + \rho_l{}^{-1/4}\right]^{-2}[g\,\sigma\,(\rho_l - \rho_v)]^{1/4} \tag{1.9}$$

where W is the width of the grooves and A_v is the area of the vapor space.

CHAPTER TWO

TEST APPARATUS

The forced convection test apparatus employed in this study was the result of a series of changes that were made to a thermal test bed originally built by Entrekin [15]. The forced convection studies conducted jointly by ASI and UAHuntsville modified Entrekin's set-up to support the higher working tube temperatures which were on the order of 200^{o}C. The apparatus used in this study is similar to that used in [1] (the SBIR final report containing a full summary of ASI's effort) with a few modifications. Since the report generated by ASI is not currently available for public release, a full description of the test apparatus is provided here for the sole purpose of providing clarity with regard to the experimental set-up. Overall, the apparatus contained a well insulated, 6 in. long evaporator section, an insulated adiabatic section, and an insulated condenser section in which a finned, 3 ft. long portion of the tube was cooled via air flow within PVC tubing (Figure 2.1). The calorimeter heat flux was measured using two sets of thermistors (upstream and downstream of the fins), and air flow measurements were taken using a hot wire anemometer at the outlet of a 6 in. diameter, 14 ft. long PVC pipe. In addition to the calorimeter, the heater temperature was used in conjunction with a power loss curve (determined as a part of this effort and described later) to measure the thermosyphon heat flux. [Note that the terms tube and thermosyphon will be used interchangeably throughout this section.]

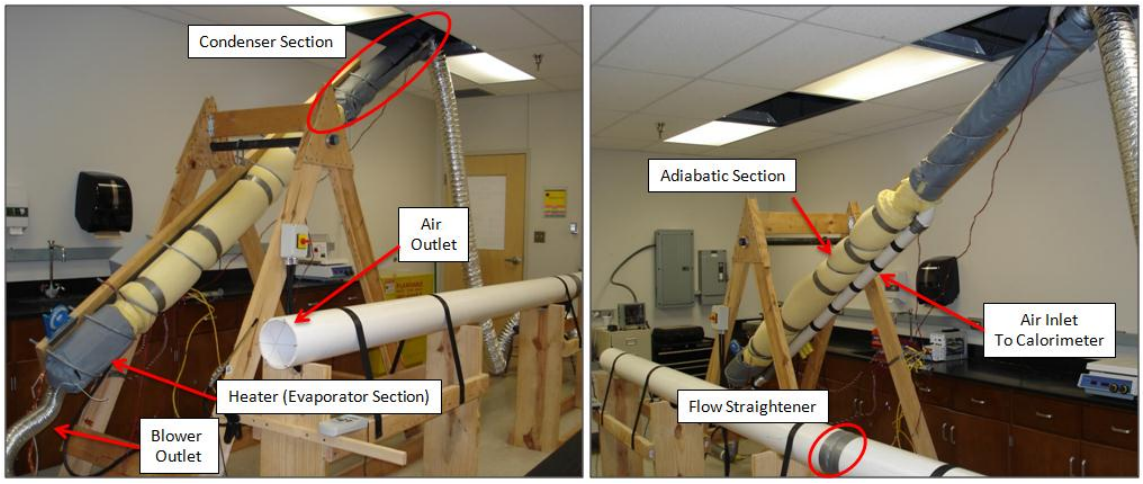

Figure 2.1: The complete test apparatus used for taking performance measurements of water and IAS-charged thermosyphons.

2.1 The Evaporator Section

Heat flux to the tubes was supplied by a coil heater (I.D. = 1 in., L = 7 in.) with a 2 KW rating (Southeastern Heaters, Inc., part No. 157CH150AX-27). A 7 in. long, concentric copper cylinder (I.D. = 11/32 in., O.D. = 1.0 in.) was used to interface the heater with the tube. The bottom portion of the thermosyphons were coated with thermal grease (AOS product No. 52030, k = 0.9 W/mK) and fully inserted into the annulus of the copper cylinder. The heater coil was covered with a cylindrical, 7 in. long tube of mineral wool insulation (I.D. = 1.375 in, O.D. = 3.375 in, McMaster-Carr part No. 9364K12), and four, 1.0 in. thick mineral wool discs were placed above the heater (Figure 2.2). An additional mineral wool disc was placed at the base of the heater. A custom made insulation jacket (Ultra Jacket series 800, Fabric Products, Inc. [*]) was wrapped around all of the components to comprise the entire heater assembly (Figure 2.2).

[*] Fabric Products, Inc. has since been acquired by Shannon Enterprises of W.N.Y. Inc.

Figure 2.2: The overall heater assembly with a 2 kW coil heater, copper tube, mineral wool insulation, and insulation jacket.

The temperature of the heater assembly was measured at the location of the coil heater using J and K-type thermocouples. A single J-type thermocouple was implanted in the heater by the manufacturer. In addition, K-type thermocouples were placed between the coils in the heater at various locations for redundancy. The exact number of K-type thermocouples placed in the coil heater changed slightly during the course of testing. For example, in the first phase of testing, a single K-type thermocouple was used in conjunction with the J-type thermocouple intrinsic to the heater (both values were averaged to obtain the heater temperature). Additional thermocouples were added in later tests to provide further redundancy. A single K-type thermocouple was also used to measure the outside temperature of the insulation jacket. This temperature was useful in estimating the convective heat loss from the insulation.

2.2 The Adiabatic Section

The temperature of the tube was measured in the adiabatic section at three different locations: 22 in., 50 in., and 78 in. as measured from the sealed end of the evaporator section. High temperature thermistors were used to measure the temperature of the water-filled tube, which was the first thermosyphon tested in the effort. Later in the study, the thermistors were damaged while interchanging the tubes. For tests conducted using the IAS-filled tube, all of the thermistors were replaced with more robust K-type thermocouples.

The heads of the respective thermistors or thermocouples were coated with thermal grease (AOS product No. 52030, k = 0.9 W/mK) and secured to the tube using kapton tape (Figure 2.3). The entire instrumented portion of the tube was wrapped in a thin sheet of fiberglass insulation. A concentric cylinder of mineral wool insulation (I.D. = 0.875 in., O.D = 2.875 in., McMaster-Carr Part No. 9364K11) was then placed around the tube (Figure 2.4). The instrumented and insulated tube was then placed in a 3 in. diameter PVC pipe. The pipe was insulated with approximately 0.75 in. of fiberglass insulation, which was then overlaid with approximately 3 in. of foam insulation (see the "adiabatic section" in Figure 2.1).

Figure 2.3: Thermistor secured to the tube with kapton tape.

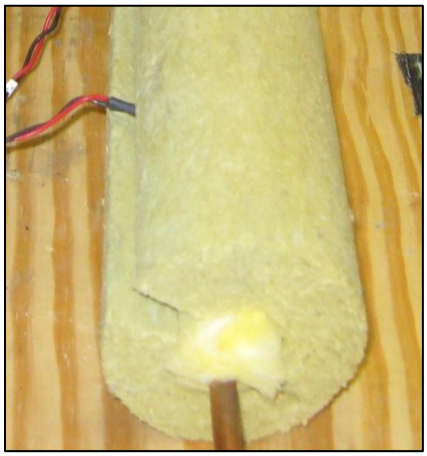

Figure 2.4: Instrumented and insulated adiabatic portion of the water and IAS-filled thermosyphons.

2.3 The Condenser Section

The PVC portions of the adiabatic section, the condenser section, and the air inlet to the calorimeter were interfaced with a PVC Wye (Figure 2.5). Three mineral wool insulation discs (2 in. thick, 3 in. diameter) were slid onto the tube above the insulated thermistor portion. Aluminum fins (0.025 in. thick, 1 in. long) were attached to the final three feet of the tube with steel wire to facilitate heat transfer in the condenser section (Figures 2.5, 2.6). The finned portion of the tube was coated with thermal grease (AOS product No. 52030) to ensure good thermal contact between the tube and fins. The 3 in. diameter PVC pipe that encompassed the fins was wrapped in approximately 3 in. of fiberglass insulation and covered with a custom made insulation jacket (see the "condenser section" in Figure 2.1). The fins were the same that were used in forced convection tests conducted by Rao in [16].

The temperature of the air upstream and downstream of the fins was measured using two pairs of thermistors. The set of the thermistors upstream on the fins were mounted on a copper L-bracket within the "air inlet" portion of the calorimeter (Figure 2.5). The thermistors downstream of the fins were mounted on two wires which were threaded across the diameter of the PVC pipe (Figure 2.5). The wires ensured minimal heat loss via conduction from the heated air to the pipe wall. Thermistors mounted on the cross wires were mounted just off the centerline. The two thermistors on the L-bracket were placed at 0.75 in. and 1.5 in. from the pipe wall, respectively.

Finally, three fine mesh aluminum screens were placed just upstream of the set of thermistors near the calorimeter outlet in an attempt to disperse and mix the heat absorbed in the air from the fins. The screens were placed on thin slices of 3 in. diameter PVC pipe and mounted in the calorimeter using a 3 inch PVC coupling (Figure 2.5). The PVC coupling was integrated into the assembly using PVC glue.

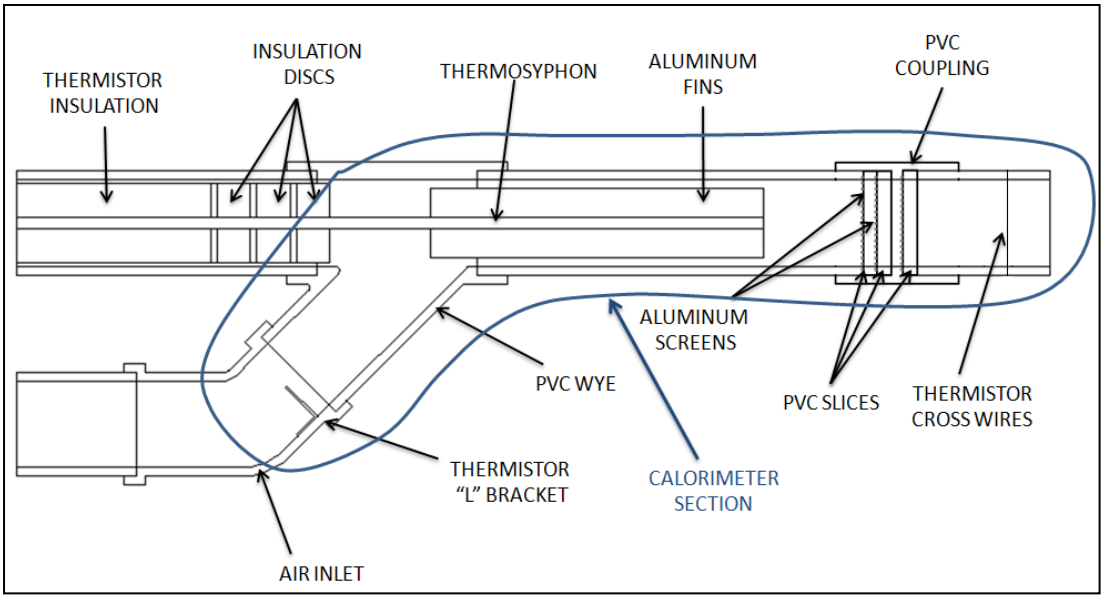

Figure 2.5: The calorimeter portion of the experimental set-up.

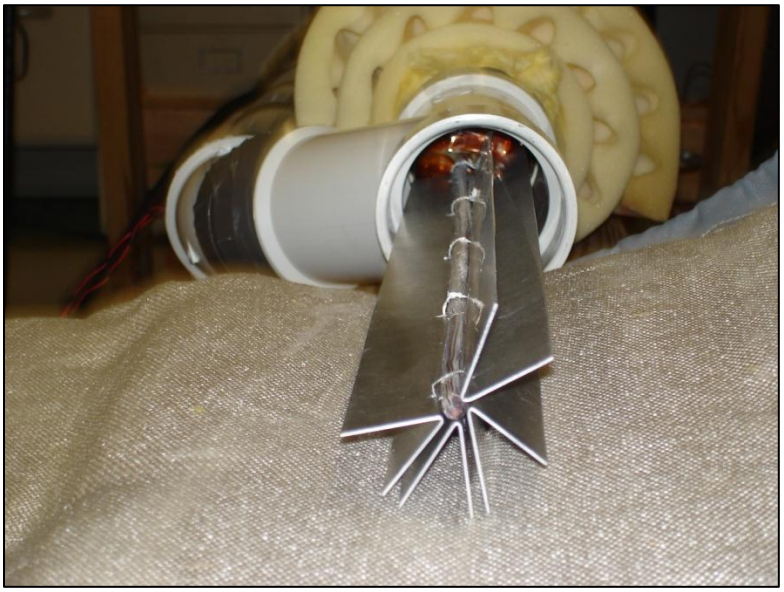

Figure 2.6: The aluminum fins which facilitated heat transfer in the condenser section of the calorimeter.

2.4 Air Flow Measurements

A reducer was used to taper the pipe diameter to six inches at the calorimeter outlet. Flex ducting then directed the air leaving the calorimeter into a 6 in. diameter, 14 ft. long PVC pipe (shown in

Figure 2.1). A honeycomb flow straightener was placed five feet from the PVC inlet in order to eliminate any oscillatory waves that may have resulted from the curved entry into the pipe. At the outlet, velocity measurements were taken using a hot wire anemometer.

A log-Tchebycheff duct traversing method was used to average 18 velocity measurements taken at marked locations at the duct outlet (Figures 2.7, 2.8). This method is equivalent to an equal area method and is designed to minimize positive error (velocity readings greater than actual) by accounting for friction losses at the duct walls [6]. The method is recommended by the ASHRAE Handbook for calculating air flow by taking an average of point velocities in a duct. Figure 2.8 shows the precise measuring points and traverse lines that are prescribed for a circular duct. For the small, 6 in. diameter PVC duct used in this study, the measurement locations for the equal area method and the log-Tchebycheff method are almost identical.

The traversing wires were slightly offset from the end of the pipe with the anemometer placed behind the wire (looking at the outlet) to take air speed measurements. This was done so the guiding wires themselves would not alter the individual point velocity measurements. The anemometer probe was attached to a flex arm which was then clamped near the PVC outlet in order to obtain steady and repeatable measurements (Figure 2.7). Duct traversing methods of this type are reported to provide velocity readings in the range of $\pm$ 3% of the total velocity [2]. In this study, three sets of velocity measurements were taken to obtain three different condenser-end heat rate calculations. These were then averaged to obtain a single calorimeter measurement for the heat rate corresponding to a particular heater input and tilt angle. The average and standard deviation for the method was 2.836 m/s and 0.011 m/s, respectively, for ten sets of measurements taken at power a level of 300 W and an angular tilt of 35^{o} from horizontal. Density and specific heat values were determined from air property tables using the air outlet temperature and an average barometric pressure of 30 inches of mercury. The temperature at the air outlet was measured at the center of the air flow using an inbuilt thermistor at the head of the hot wire anemometer.

Figure 2.7: The air outlet with marked locations for taking velocity measurements using the log-linear duct traversing method.

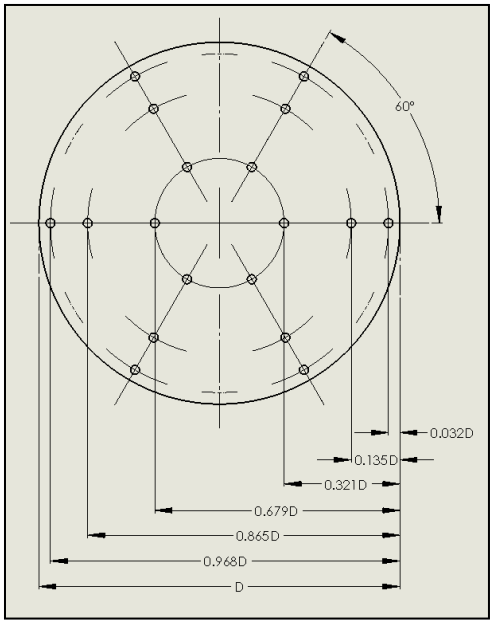

Figure 2.8: Measuring points and traverse lines used to take velocity measurement with an anemometer using a log-Tchebycheff duct traversing method.

Air flow was generated using a 7.5 Amp Craftsman electric blower with a 150 mph air outlet capacity. The flow into the air inlet portion of the apparatus was controlled using a 3.0 in. diameter PVC pipe that was attached to the blower outlet. Holes were drilled in the top of the pipe to reduce the air

speed such that tube temperatures of 200^{o}C were attained with heater input levels of 700 W or higher (Figure 2.9). The blower was joined to the calorimeter inlet pipe with 3.0 in. diameter flex tubing which was sealed at both ends with copious amounts of duct tape.

Figure 2.9: An air flow supply consisting of an electric blower and adjoining tubing.

2.5 Thermosyphons

The thermosyphons tested in this study were 5/16 in. in diameter and 10 ft. long. Both the water and IAS-filled thermosyphons that were originally considered for this study had been tested previously in the joint effort conducted by ASI and UAHuntsville [1]. Both tubes contained small, helical grooves along the inner wall. The IAS-filled tube, however, showed signs of a pin-hole leak and had to be discarded. A similar 5/16 in. diameter tube that had been tested previously in UAHuntsville studies [22] was used in its place. Although the new IAS-filled tube lacked the helical grooves innate to the water tube, it had the same length and outer diameter, and thus was still considered a viable option for a performance comparison. Figure 2.10 shows a picture of the helical grooves of the water-filled tube as well as a view of

the cross section. The dimensions associated with the groove geometry are given in Table 2.1. The tubes were purchased from Wolverine Tube, Inc. (catalog No. 36-23121208). The internally grooved thermosyphons were charged with a liquid volume of approximately 15 mL.

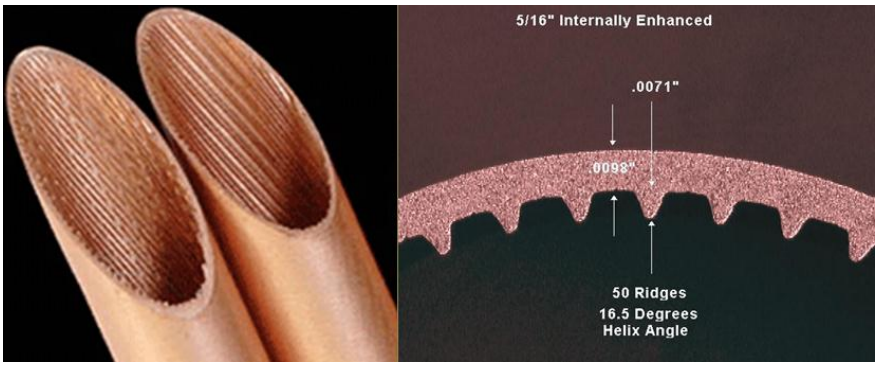

Figure 2.10: A picture of the thermosyphon internal helical grooves[†].

Table 2.1: Dimensions of the grooved thermosyphon used in this study.

Grooved Thermosyphon Dimensions	
Outside Diameter	.3125" Nominal – Average +/- .002"
Bottom Wall Thickness	.0117" +/- .0.001" At-A-Point
Ridge Height (Fin Height)	.008" +/- .001" At-A-Point
Bottom ridge length	0.007"
Top ridge width	0.003"
Flat between ridges	0.011"
Helix (Lead Angle)	18 Degrees +/- 3 Degrees
Number of Grooves	50

[†] Graphics supplied by Wolverine Tube, Inc.

CHAPTER THREE

CALORIMETER UNCERTAINTY ANALYSIS

The uncertainty of a nearly-identical calorimeter set up was estimated by ASI in [1]. That study implemented a Monte Carlo simulation to determine the uncertainty of the calorimeter readings using the following data reduction equation (DRE):

$$Q_{cal} = (dm/dt)_{air} C_p \Delta T$$

$$Q_{cal} = \rho_{air} A_{pvc} V_{exit} C_p (T_{out} - T_{in}) \quad (3.1)$$

In Equation 3.1, the V_{exit} and $(T_{out} - T_{in})$ terms were the primary measured values, and considered to be the main sources of uncertainty. In contrast, the uncertainty associated with the ρ_{air} and C_p terms were considered to be negligible, as they were tabulated values based on the outlet air temperature. In this study, a separate and unique Monte Carlo analysis was completed using the same basic assumptions. The new analysis is warranted since the method of measuring the heat rate is slightly different from that performed by ASI (the heat rate is found using three sets of calorimeter measurements as opposed to only one, as was done in that study).

On a final note, an analysis of the density and specific heat values determined from the temperature at the air outlet indicates that errors associated with each of these values is indeed negligible. The temperature at the outlet varied by approximately 5^{o}C between the 300 W and 700 W heater input levels for the water tube, corresponding to a 1.6% and a 0.29% variation in the ρ_{air} and C_p values, respectively. Thus, the uncertainty in ρ_{air} and C_p associated with *uncertainty* in the air outlet temperature measurement (which would be on the order of 0.1 ^{o}C) is indeed very small. As previously mentioned, the ρ_{air} and C_p values were found using a barometric pressure of 30 in. Hg, which is very close to the average barometric pressure for Huntsville, AL [24]. That barometric pressure remains relatively

constant with a *maximum* variation of 1.33 inches of mercury observed over a 5 year period [24]. The normal monthly variations are much smaller, on the order of 0.5 inches of mercury, which corresponds to a density variation of about 1.7%. Assuming that variation corresponds to a 95% confidence interval, the corresponding error in the calorimeter heat rate determined by a Monte Carlo uncertainty analysis is on the order of 0.2%.

3.1 Uncertainty of the Calorimeter Thermistors

The overall uncertainty of the thermistor elements located upstream and downstream of the fins is estimated in this section. Each thermistor had a specified 0.2 ^{o}C tolerance across their entire temperature range. This value was assumed to be the systematic uncertainty innate to each thermistor element. In addition, a temperature difference which was higher than 0.2 ^{o}C was observed between the thermistors located upstream of the fins. The cause of the additional variation was attributed to incomplete distribution of absorbed energy in the air flow coupled with the distinct locations of the thermistors at the outlet. Furthermore, the temperature difference increased at higher power levels when the tube dissipated more energy into the calorimeter. There was an attempt to quantify the variation in an additional uncertainty estimate, but the analysis yielded heat rate uncertainties for the calorimeter that were overly conservative. No variation beyond 0.2 ^{o}C was observed between the thermistors at the air inlet.

The effect of averaging the two temperature values at both locations was found using the Taylor series method. Equation 3.2 shows the data reduction equation (DRE) for averaging the thermistor values and Equation 3.3 shows corresponding Taylor series uncertainty equation. A simplified form of the equation is shown in Equation 3.4 (derived by taking the partial derivatives of Eq. 3.3). The values of U_{T1} and U_{T2}, which are the uncertainties associated with T1 and T2 for a 95% confidence interval, were both assumed to be 0.2 m/s (the systematic uncertainty of each thermistor). Using Eq. 3.4, the value for U_{Tave} is 0.141 m/s.

$$T_{ave} = (T_1 + T_2)/2 \tag{3.2}$$

$$U_{Tave}^2 = (\partial T_{ave}/\partial T_1)^2 \cdot U_{T1}^2 + (\partial T_{ave}/\partial T_2)^2 \cdot U_{T2}^2 \tag{3.3}$$

$$U_{Tave}^2 = (1/2)^2 \cdot U_{T1}^2 + (1/2)^2 \cdot U_{T2}^2 \tag{3.4}$$

3.2 Uncertainty of the Velocity Measurements

Velocity measurements were obtained using a log-Tchebycheff duct traversing method which was identical to that used by ASI/UAHuntsville in [1]. The uncertainty of the velocity measurements stem from the manufacturer tolerances for the anemometer, as well as placement errors that might have occurred while taking measurements. Those placement errors originate from three main sources [1]:

1. The uncertainty associated with the inexact markings on the traversing lines
2. The uncertainty associated with the angles of the traversing lines
3. Uncertainties that stem directly from incorrectly placing the hot wire anemometer while taking individual velocity measurements

With the placement and handling errors assumed negligible, the study in [1] generated estimates for the systematic and random uncertainties for the velocity measurements that are applicable to this effort. The systematic uncertainty for the anemometer was estimated using an accuracy percentage specified by the manufacturer, which corresponding to an uncertainty of approximately 0.3 m/s [1]. Since the duct traversing, log-Tchebycheff method is accurate to $\pm$ 3% of the total velocity measurement, average air flow measurements from [1] (about 3.0 m/s, which is very close to the velocities measure in this study) were used to determine the random uncertainty. That value was found to be 0.09 m/s. The root-mean-square of the systematic and random uncertainty values gave an overall uncertainty estimate of 0.313 m/s [1]. The uncertainties associated with the velocity readings that were determined in [1] were assumed to remain the same in this study.

3.3 Monte Carlo Uncertainty Analysis

A Monte Carlo uncertainty analysis was conducted using the overall uncertainties associated with the anemometer and calorimeter thermistors. The analysis was conducted using 10,000 random numbers which were generated assuming a normal distribution. The analysis employed constant values for A_{pvc}, V_{exit}, and C_p (referring back to Eq. 3.1). The resulting 95% confidence uncertainty estimate of a single calorimeter heat rate measurement is $\pm$ 87.62 W (approximately 12.5% of a heater input of 700 W).

Since three sets of heat rate measurements were averaged to obtain a single calorimeter measurement, the uncertainty analysis was extended to account for the effects of averaging. Equation 3.5 shows the DRE for averaging the heat rate measurements. Equation 3.6 shows the corresponding Taylor series equation. Equation 3.7 shows the further-simplified Taylor series equation with the solved partial derivatives from Eq. 3.6. Using the equations below, the overall uncertainty for the averaged heat rate measurement is approximately $\pm$ 50.58 W (about 7.2% of a heater input of 700 W).

$$Q_{ave} = (Q_1 + Q_2 + Q_3)/3 \tag{3.5}$$

$$U_{Qave}^2 = (\partial Q_{ave}/\partial Q_1)^2 \cdot U_{Q1}^2 + (\partial Q_{ave}/\partial Q_2)^2 \cdot U_{Q2}^2 + (\partial Q_{ave}/\partial Q_3)^2 \cdot U_{Q3}^2 \tag{3.6}$$

$$U_{Qave}^2 = (1/3)^2 \cdot U_{Q1}^2 + (1/3)^2 \cdot U_{Q2}^2 + (1/3)^2 \cdot U_{Q3}^2 \tag{3.7}$$

3.4 Uncertainty Verification Test

In an effort to estimate the overall *random* uncertainty of the calorimeter and verify the estimates determined in the previous section, a total of ten heat flux measurements were taken using the water-filled tube with 300 W applied to the heater. The measurements were taken on two separate occasions (four measurements taken one day, six taken on another). At both times the device was allowed to reach steady-state (the time to achieve steady state was determined by experiment and is described later) and a series of heat flux measurements were subsequently taken. The ten heat flux measurements are shown in Figure 3.1. The spread was relatively small compared to the uncertainty

estimates in the previous section, with a standard deviation of 1.67 W. This corresponds to a 95% confidence interval of approximately $\pm$ 3.77 W (or 1.3% of the 300 W supplied to the heater).

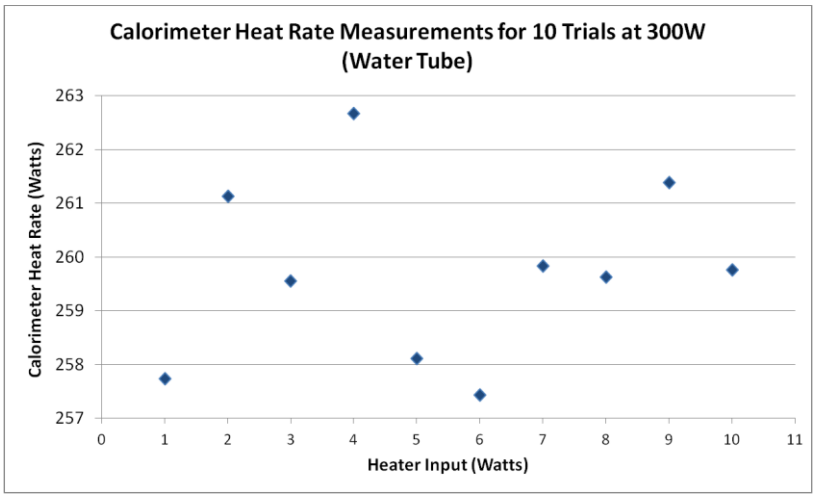

Figure 3.1: Calorimeter Heat Rate Measurements for 10 Trials at 300 W.

One reason for the small spread of the actual data measurements is that there was a very low variation in the corresponding velocity measurements. For example, the thirty separate velocity measurements (three for each heat rate value plotted in Figure 11) had standard deviation of 0.0193 m/s, which corresponds to a 95% percent confidence interval of $\pm$ 0.0395 m/s. This value could be considered the random uncertainty associated with the velocity measurements, and it is close to the random error associated with the duct traversing method (0.09 m/s). If the value of 0.0395 m/s is incorporated into a Monte Carlo analysis as the uncertainty for the anemometer, the heat rate uncertainty reduces to $\pm$ 13.41 W. This shows that the systematic uncertainty of 0.3 m/s for the anemometer contributes greatly to the more conservative heat rate uncertainty estimate of $\pm$ 50.58 W that was found earlier. This also shows that the calorimeter is useful for comparative purposes, since the spread attributed to random uncertainty is small.

CHAPTER FOUR

PERFORMANCE ESTIMATES USING THE HEATER TEMPERATURE

An additional method of determining the performance of the water and IAS-filled thermosyphons was desired to confirm the heat rate measurements of the calorimeter, and to attain more accurate heat rate measurements with a lower overall uncertainty. To this end, the heat rate losses from the heater package and the adiabatic section were determined to generate an estimate for the heat lost from the tube in the condenser section. Equation 4.1 shows the fundamental equation used to determine the heat rate dispersed in the finned portion of the tube. As will be shown later, this method proved to provide an extremely accurate measurement of thermosyphon performance.

$$Q_{condenser} = Q_{in} - Q_{loss\_heater} - Q_{loss\_adiabatic} \tag{4.1}$$

4.1 Power Lost From the Heater

The analysis to determine the rate of heat loss through the heater insulation was conducted to: 1) determine the rate at which heat is transported from the heater by the tube, and 2) verify the calorimeter heat rate measurements. The following equation was used as a starting point to determine the energy lost by the heater:

$$Q_{in} = Q_{tube} + Q_{lost} \tag{4.2}$$

Where Q_{in} is the heat rate supplied by the heater, Q_{tube} is the heat rate carried from the heater assembly by the tube, and Q_{lost} is the heat rate lost through the insulation surrounding the heater. If the tube is removed from the heater assembly, then Eq. 4.2 becomes the following:

$$Q_{in} = Q_{lost} \tag{4.3}$$

where the power supplied by the heater necessarily becomes the heat rate lost through the surrounding insulation. If the temperature of the heater is measured at various Q_{in} values with the tube removed from the heater assembly, then a correlation between the heater temperature and the heat lost through the surrounding insulation can be found. This method was used by both Entrekin and Rao ([15], [16]) and implemented in this study.

A small, hollow tube with a 5/16 in. diameter was inserted into the copper annulus of the heater assembly. The heater assembly was then secured onto the rotatable test frame apparatus and oriented at 35 degrees (Figure 4.1). The heater temperature was measured using J and K-type thermocouples (one of each). The J-type thermocouple had been implanted in the heater by the manufacturer, and the K-type thermocouple was placed between the coils of the heater at the center of its length. An additional K-type thermocouple measured the ambient temperature.

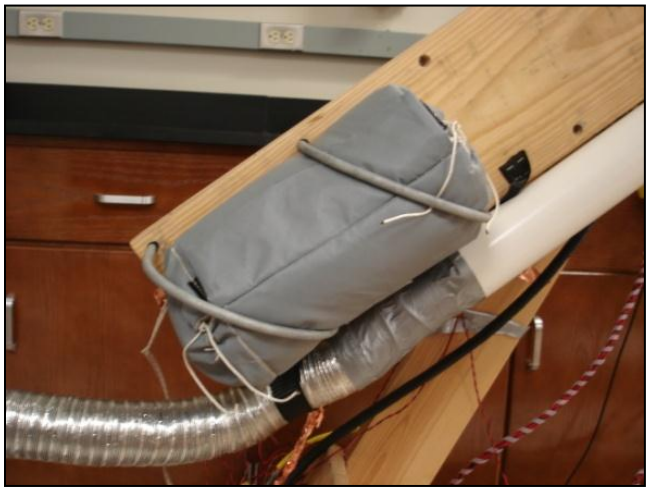

Figure 4.1: The heater assembly oriented at 35 degrees to conduct the heat loss test.

The time needed to achieve steady state operation was determined by recording the heater temperature while increasing the power supplied from 10 to 34 Watts. The rises in average temperature of the coil heater and the insulation temperature were then recorded as a function of time. Figure 4.2

shows the transient temperature rise corresponding to each of the measured temperatures. Overall, the plots show that approximately 7 hrs. was needed for the heater to reach a steady state operating temperature in this particular configuration.

To determine the heat lost as a function of power applied to the heater, the heater temperature was recorded for a series of power levels. That plot is shown in Figure 4.3, where the power supplied is plotted against the difference between the heater temperature and ambient temperature. Since the heater temperature approached the temperature limit of the surrounding mineral wool insulation at higher power levels, three additional temperature measurements were taken at 10, 35, and 60 Watts to confirm that the thermal resistance of the insulation had not changed. As shown in the figure, that set of "confirmation data" did not vary from the original curve.

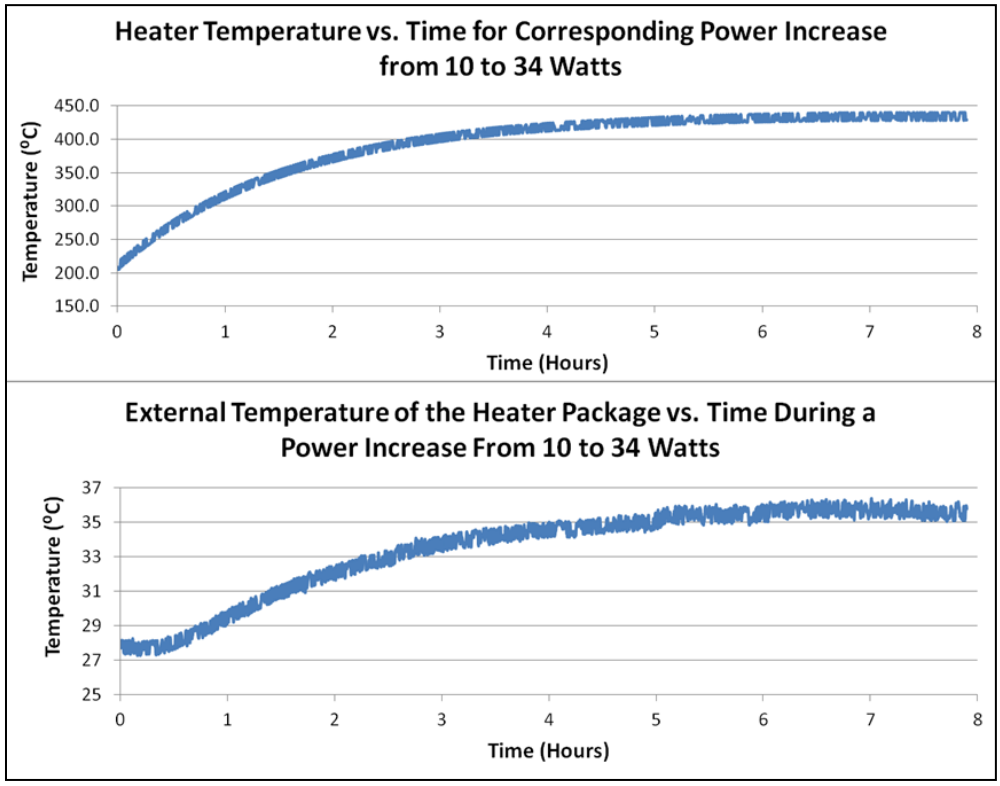

Figure 4.2: The rise in the temperatures of the heater coil and insulation package corresponding to a heater input of 10 to 34 Watts.

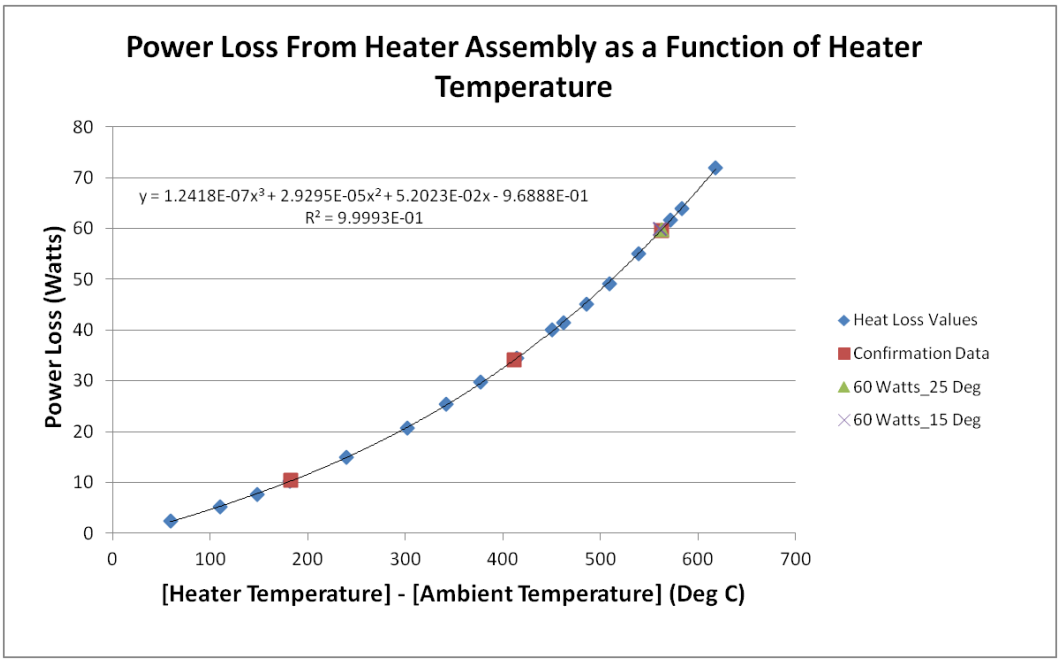

Figure 4.3: Power lost from the heater assembly as a function of heater temperature.

Additionally, there was a desire to get a "feel" for the overall sensitivity of the power loss curve due to the angular variation of the heater assembly. To that end, the heater temperature was measured at a power input of 60 Watts at angular inclinations of 25 and 15 degrees from horizontal (the same angles at which the thermosyphon performance was measured). As shown in Figure 4.3, the data points corresponding to the different angles fall directly on the original curve. This point is further emphasized with close-up view of that portion of the data plot (Figure 4.4).

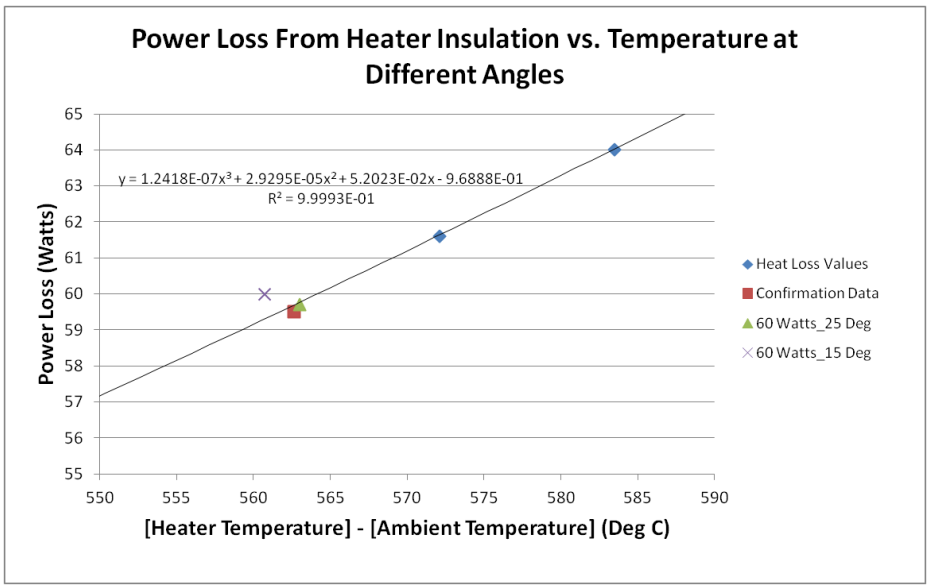

Figure 4.4: A close-up view of the power loss curve in the portion corresponding to the measurements taken at 25 and 15 degrees.

4.2 Closed Form Analysis to Confirm Negligible Changes in Heat Loss with Angular Variation

An additional closed form analysis was completed to confirm a low amount of variation of the predicted rates of heat loss with angular variation. Specifically, the difference in the rate of heat loss was analytically found for horizontal and vertical cylinders containing the same overall dimensions of the heater assembly. The equations used to determine the film coefficients can be found in [7]. Heat loss for the cylinder in the vertical position was found by finding the film coefficient for a vertical flat plate. The total rate of heat loss was then found using circumferential area of the cylindrical insulation jacket. Such an approach was considered adequate in [7] to model the heat loss through a large vertical cylinder. In the vertical orientation, heat loss through the ends was modeled using natural convection equations for a heated horizontal plate facing upward and downward, respectively. For modeling the heat loss of the heater in a horizontal configuration, natural convection equations for a horizontal cylinder were used. In the horizontal orientation, heat loss through the ends was estimated by using the aforementioned natural convection equations for a vertical plate. Finally, radiation was also accounted for while modeling the rate of heat loss in both vertical and horizontal orientations.

The natural convection coefficient for a vertical plate (which was extended to apply to a vertical cylinder) was found using the following set of equations:

$$\Psi = [\, 1 + (0.492/Pr)^{9/16}]^{-16/9} \tag{4.4}$$

$$Ra_L = \beta\, \Delta T\, g\, L^3\, Pr/\nu^2 \tag{4.5}$$

$$Nu_L = 0.68 + 0.670\, (Ra_L \Psi)^{1/4} \tag{4.6}$$

$$h_f = (k/L)\, Nu_L \tag{4.7}$$

$$Q = h_f A\, (T_s - T_{amb}) \tag{4.8}$$

where Ψ is termed the "Prandtl number function", Pr is the Prandtl number, Ra_L is the Rayleigh number for laminar flow, L is the length of the flat plate, Nu_L is the Nusselt number, β is the inverse of the reference temperature, ΔT is the difference between the surface and ambient temperatures, g is the gravitation constant, ν is the kinematic viscosity, h_f is the natural convection film coefficient, A is circumferential area of the cylinder, and Q is the rate of heat transfer. The film coefficient found by using (4.7) was also used to find the heat loss through the ends of the cylinder in the horizontal configuration. In this case, the area used in (4.8) was the cross sectional area of the entire cylindrical heater assembly.

For a horizontal cylinder, the laminar Nusselt number becomes the following:

$$Nu_D = 0.36 + 0.518\, Ra_D^{1/4}/[1 + (0.559/Pr)^{9/16}]^{4/9} \tag{4.9}$$

$$h_f = (k/D)\, Nu_L \tag{4.10}$$

where Ra_D is the Rayleigh number based on the diameter of the cylinder, and h_f is the diameter-dependent film coefficient. The Rayleigh numbers found for the horizontal and vertical cases were relatively small. The listed Nusselt equations for the vertical plate and horizontal cylinder correspond to the appropriate ranges of Raleigh numbers that were applicable in this analysis.

The average Nusselt number of a heated horizontal plate facing down and up was determined using Equations 4.11 and 4.12, respectively. In both equations, the term Ra_L is the Raleigh number for a square plate with sides of length 'L'. In this analysis, Ra_L was estimated using the diameter of the heater insulation jacket.

$$Nu_{L,ave} = 0.82\ Ra_L^{1/5} \tag{4.11}$$

$$Nu_{L,ave} = 0.54\ Ra_L^{1/4} \tag{4.12}$$

A surface temperature of 36^{o}C was assumed in the study and corresponds to the outer temperature of the insulation package with 34 W supplied to the heater (Fig. 4.2). The ambient temperature was assumed to be 20^{o}C. The diameter of the cylinder used in the analysis was 6.325 in., and the length was 11 in. (the approximate dimensions of the heater insulation jacket). The surface of the insulation jacket was assumed to have an emissivity of 0.8 for estimating the rate of heat loss due to radiation. The heat loss estimates for the cylinder in the vertical and horizontal positions were 26.79 W and 25.53 W, respectively. This corresponds to a difference of 4.7%.

The heat loss estimates are slightly smaller than the 34 W needed to produce an equivalent 36^{o}C surface temperature by experiment. However, the natural convection analysis above does not account for air movement within the insulation materials internal to the heater package, wrinkles and edges in the insulation jacket, and the coupling of heat transfer effects that may occur between the adjacent surfaces of the insulation jacket. Overall, the analysis showed a small variation (4.7%) in the estimated rate of heat loss between the vertical and horizontal configurations. The deviation is larger than the observed change in heat rate between 35 and 15 degrees that was observed experimentally. This may be caused in part to the vertical plate assumption that was applied to a cylinder in the 90 degree orientation. Overall, the small variation confirms that assuming a negligible difference in the rate of heat loss between the orientations of 35 and 15 degrees from horizontal is completely reasonable.

4.3 FEA Analysis to Confirm the Time to Achieve Steady State

A finite element analysis was conducted to confirm the observed temperature rises in the heater. A three dimensional model was made of the heater assembly that accounted for the annular copper rod, the heater coils, the insulation materials, and the copper tube that replaced the thermosyphon in the power loss analysis (Figure 4.5). The coil heater was represented by an annular steel cylinder having the same length and inner and outer diameters. Standard properties for copper were used for the copper rod and tube, and the heater was given standard properties for steel. The insulation jacket was modeled as fiberglass insulation. The density and specific heat values used to model the mineral wool and fiberglass materials are shown in Table 4.1. The thermal conductivity of both materials was modeled as a function of temperature using temperature-dependent information obtained from [31]. A heat rate boundary condition of 34 Watts was applied to the inner and outer surfaces of the concentric cylinder that was used to model the heater. In addition, a natural convection boundary condition of 4 W/cm^2K was applied to the entire outer surface of the insulation jacket. This value is very close to the film coefficient that was found using natural convection equations in the previous section. A radiation boundary condition was also applied to the external surfaces of the insulation jacket with an assumed emissivity value of 0.8. The initial temperature of all of the components of the model, as well as the ambient temperature, was set to 20^oC.

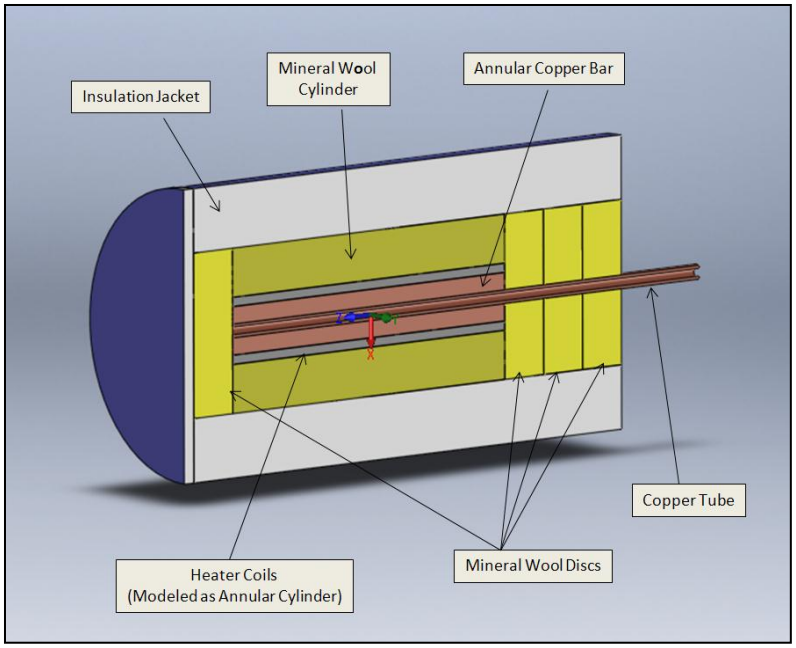

Figure 4.5: The three dimensional configuration used to model the transient temperature rise in an FEA analysis.

Table 4.1: The properties of mineral wool and fiberglass used in the FEA analysis

Property	Mineral Wool	Fiberglass
Density (kg/m^3)	150	10
Specific Heater (J/kg-K)	835	840

Figure 4.6 shows a plot of the maximum heater temperatures spanning an eight hour transient FEA analysis of the heater assembly. As shown in the figure, the overall time to steady state is nearly identical to what was observed experimentally in Figure 4.2. The final heater temperature corresponding to the 34 W heat input is higher than that observed for the same wattage on the power loss curve by about 285°C. This is most likely due to natural convection effects internal to the heater package that would be difficult to account for in an FEA model. Figure 4.7 shows the distribution following the eight hour transient analysis. The results confirm that the time to steady state observed during the experimental analysis is reasonable.

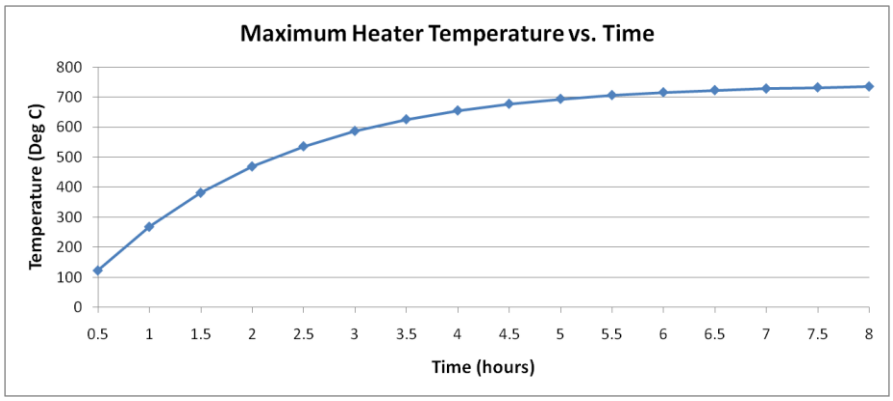

Figure 4.6: A plot of the maximum heater temperature vs. time for a transient, three dimensional FEA analysis of the heater.

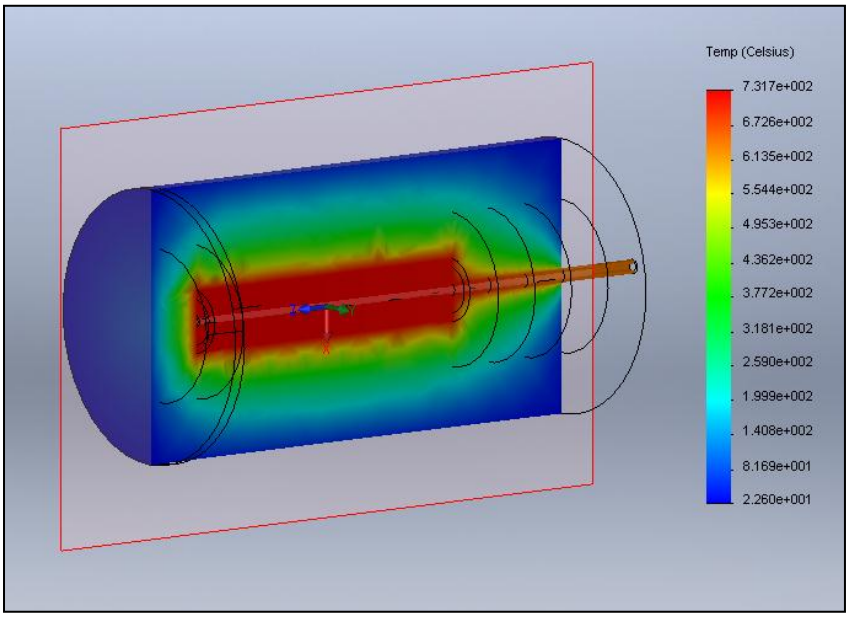

Figure 4.7: The temperature distribution in the heat package following an eight hour transient FEA analysis.

4.4 Uncertainty of the Power Loss Curve

An attempt was made to estimate the uncertainty associated with the power loss curve using actual experimental data. Ideally, with a specific amount of power applied to the heater, the tube would be allowed to reach steady state multiple times, with the heater temperature corresponding to each of the different trials being recorded. The standard deviation of the temperature could then be used to

estimate total uncertainty of the power lost through the surrounding insulation. This is done by applying a Taylor series analysis to the trendline polynomial equation of the power loss curve (Figure 4.3).

While multiple start-up tests were not conducted at any single power level, the heater temperature was measured at three different angles (35, 25, and 15 degrees) for input power levels of 300 W, 450 W, and 600 W. Furthermore, the thermosyphon performance was shown to be relatively independent of the inclination angle, with nearly constant heater temperatures observed across the angular range (discussed later). Taking the standard deviation of the temperatures measured at the three **a**ngles corresponding to a specific power input was thought to provide a conservative uncertainty estimate of the heater temperature, which could then be used in conjunction with the Taylor series method to find the overall uncertainty of the power loss curve. The polynomial curve fit for the power loss curve is shown in Equation 4.13. Equation 4.14 shows the corresponding Taylor series equation. Equation 4.15 shows the equation with the derivative calculated from Equation 4.14. The standard deviation of the three heater temperatures recorded at 600 W was 4.04 ^{o}C, which correlates to a 95% confidence interval of $T_{600W} \pm 9.51\ ^{o}C$. A conservative power loss uncertainty estimate generated from the Taylor series method using a value of T = 579.2 (the average value of the three temperature measurements) is then $Q_{loss} \pm 2.0$ W. The analysis shows that the experimentally derived power loss curve provides an accurate means to determine the total amount of heat flux carried by the tube.

$$Q_{loss} = (1.242)(10^{-7})\,T^3 + (2.930)(10^{-5})\,T^2 + (5.202)(10^{-2})\,T - 0.968 \tag{4.13}$$

$$U_{Qloss}^{\ 2} = (dQ_{loss}/dT)^2 \cdot U_T^{\ 2} \tag{4.14}$$

$$U_{Qloss}^{\ 2} = [(3.726)(10^{-7})\,T^2 + (5.86)(10^{-5})\,T + (5.202)(10^{-2})]^2 \cdot U_T^{\ 2} \tag{4.15}$$

4.5 Heat Loss in the Adiabatic Section

A simple 2-D thermal analysis was used to estimate the rate of heat loss from the adiabatic section. Figure 4.8 shows a cross-sectional schematic of the adiabatic section with overall dimensions, as well as the thermal conductivities of each of the cross-sectional layers. A natural convection coefficient

for the outer diameter of the foam insulation was determined using the natural convection equations for a horizontal cylinder (described earlier) with a length of 72 in. and an outer diameter of 10.5 in. The measured ambient air and foam surface temperatures were used to determine the natural convection coefficient at each heat level. Table 4.2 shows tube temperatures and corresponding rate of heat loss for heater inputs of 300 W, 450 W, 600 W, and 700 W (at a 35 degree incline) for the water and IAS-filled tubes. There is a lack of data for the IAS-filled tubes beyond 450 W because the tube showed signs of burnout for higher heat rates.

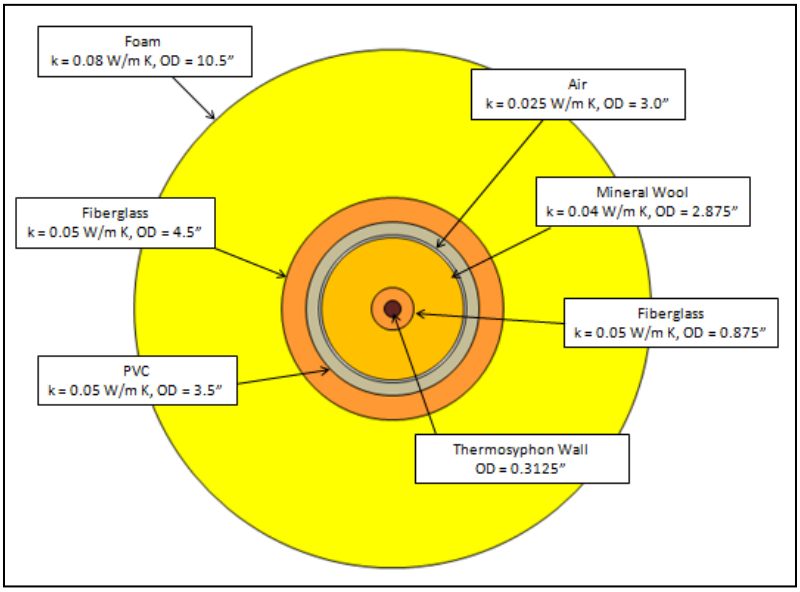

Figure 4.8: A cross sectional view of the insulating layers in the adiabatic section.

Table 4.2: Heat loss estimates in the adiabatic section corresponding to the operating temperatures of the water and IAS-filled tubes.

Water-Filled Thermosyphon				**IAS -Filled Thermosyphon**			
Tube Temperatures				**Tube Temperatures**			
Heat Input (W)	35 Deg	25 Deg	15 Deg	Heat Input (W)	35 Deg	25 Deg	15 Deg
300	107.6992	107.6036	107.2049	300	105.57	107	107.2
450	145.2455	145.6766	145.7351	450	138.93	138.54	139.72
600	180.4327	178.4221	178.04				
700	197.6635						
Heat Loss Through the Adiabatic Section				**Heat Loss Through the Adiabatic Section**			
Heat Input (W)	35 Deg	25 Deg	15 Deg	Heat Input (W)	35 Deg	25 Deg	15 Deg
300	12.97667	12.88126	12.7775	300	12.65357	12.86462	12.80635
450	19.15164	19.15342	19.14361	450	18.01774	17.89113	17.98589
600	24.76475	24.45776	24.39637				
700	27.70035						

CHAPTER FIVE

THERMOSYPHON TESTING

Heat was applied to the heater coils gradually to reach the target heat input value. Typically, each test began by applying 100 W to the heater coils, waiting until the tube temperature had reached approximately 100^{o}C, and then applying 300 W to the heater coils. The power applied to the heater was then increased if the test was to be conducted using a higher power level. Once the appropriate power level for the test was applied to the heater, the apparatus was allowed to come to steady state before taking measurements.

The time to steady state operation was determined by recording a rise in the heater temperature, the temperature of the tube, and the outer temperature of the heater package for a power input value of 450 W. At time t = 0, 100 W was applied to the heater. When the tube temperatures reached 100^{o}C, the heater power was increased to 450 W. This was done for both the water and IAS-filled thermosyphons. Data for the IAS tube is shown in Figure 5.1. From the time that 450 W was applied to the heater, the tube and heater required approximately two hours to reach steady state operation in the forced convection apparatus. Consequently, a time period of two hours was allowed for each tube to achieve steady state at the various angle and power level combinations that were tested.

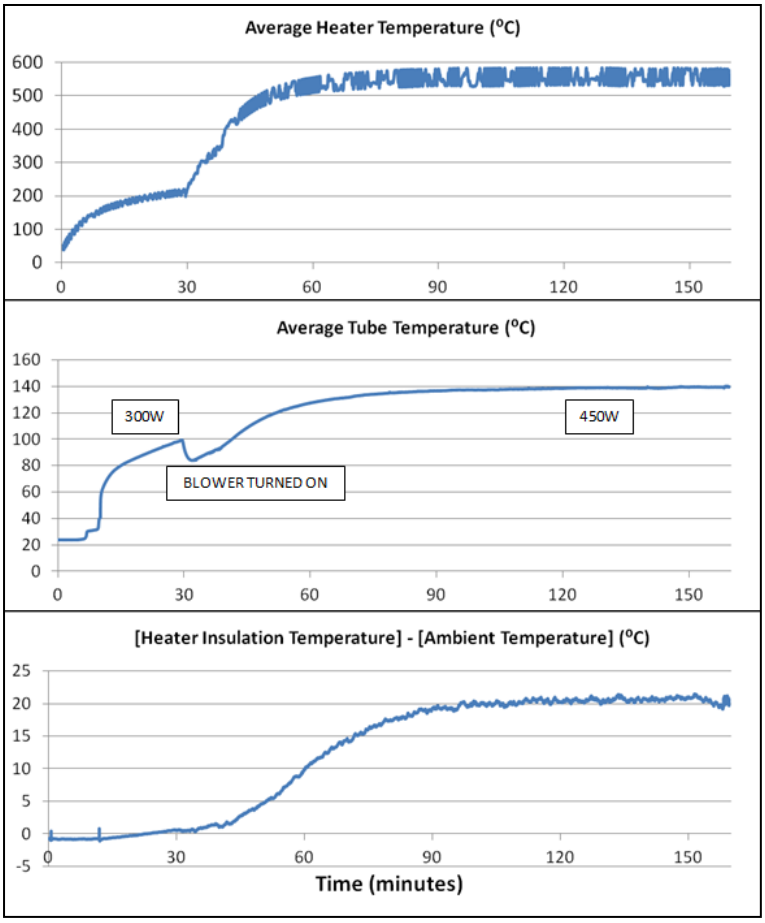

Figure 5.1: Plots showing the temperature rise of the average heater and tube temperatures from t = 0 to steady state operating temperatures at 450W.

Once the tube had reached steady state at a particular power input and tilt angle, three sets of calorimeter measurements were taken and averaged. While velocity measurements were being taken for each set of calorimeter measurements (18 distinct values using the duct traversing method), the temperatures of the heater, the heater insulation, the tube, as well as the calorimeter inlet and outlet temperatures were measured. The data was taken at a rate of 50Hz. Those temperatures were then averaged over the span of time that was required to take the single set of velocity measurements (about 8 min.). The measured tube temperatures were used later to provide a heat loss estimate for the adiabatic section, and the calorimeter inlet and outlet temperatures were used to determine the heat absorbed by the air in the calorimeter.

Since the variac controller caused a good deal of noise in the temperature readings of the heater coil (see the plots of the heater temperature in Figure 5.1), the controller was turned off momentarily after recording the data associated with the calorimeter measurements. The data acquisition rate was increased to 1.2kHz while recording the heater temperature so that any trace amounts of noise could be observed in a data plot. Figure 5.2 shows a temperature plot for a heater thermocouple when the variac controller was momentarily turned off to obtain a temperature reading. In the plot, the variac was turned off at approximately t = 0.5 sec., and back on again just after t = 1.5 sec. As shown, this method effectively reduced the noise in the temperature measurements and allowed for data to be taken before any noticeable drop in the heater temperature could occur.

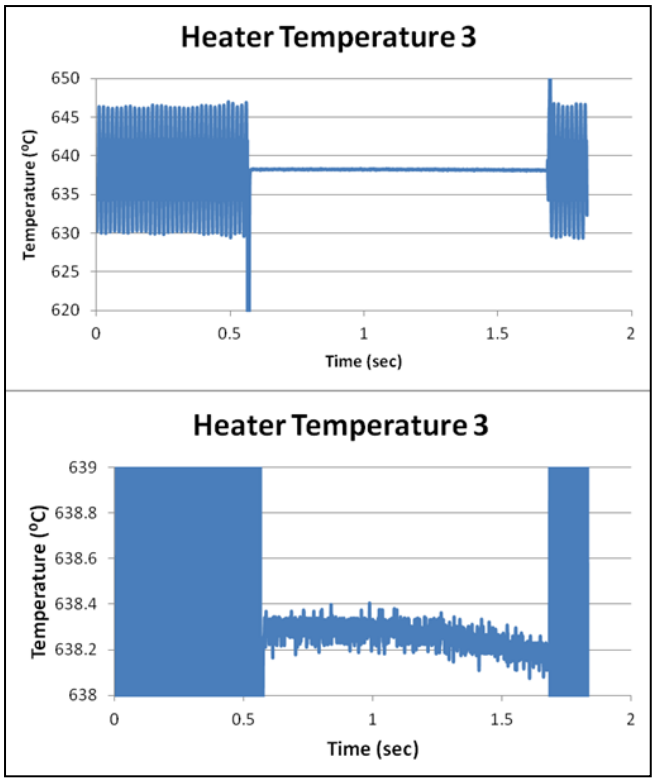

Figure 5.2: The temperature recording for a single thermocouple located between the coils in the heater section with the variac controller momentarily turned off.

CHAPTER SIX

RESULTS

6.1 Water-Filled Thermosyphon

The condenser-end heat rates for the water-filled tube that were measured using both the calorimeter and the heater power loss curve are plotted in Figure 6.1. Overall, heat rate measurements using both methods yielded similar results. The curve was highly linear with little variation in performance with angular tilt. This becomes especially evident with a close up look at the spread for each power level. Figure 6.2 shows the variation in heat rate measurements at each power input setting. As shown in the figure, heat rate estimates using the heater temperature (labeled xxDeg_Est in the legend) showed an extremely low amount of variation with angular tilt. Finally, Figure 6.3 shows the heat flux carried by the tube from the heater as determined from the power loss curve. Of course, this ignores the heat loss in the adiabatic section and solely quantifies the amount of heat carried away from the heater.

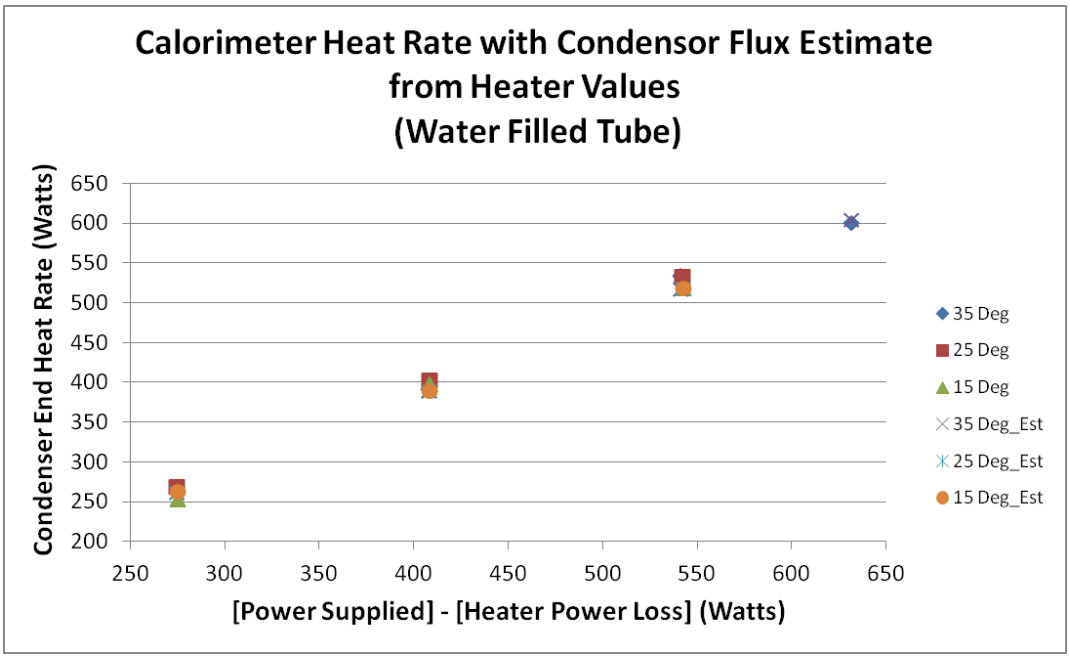

Figure 6.1: The condenser end heat rate for the water-filled tube measured using the calorimeter heat rate and the power loss curve for the heater.

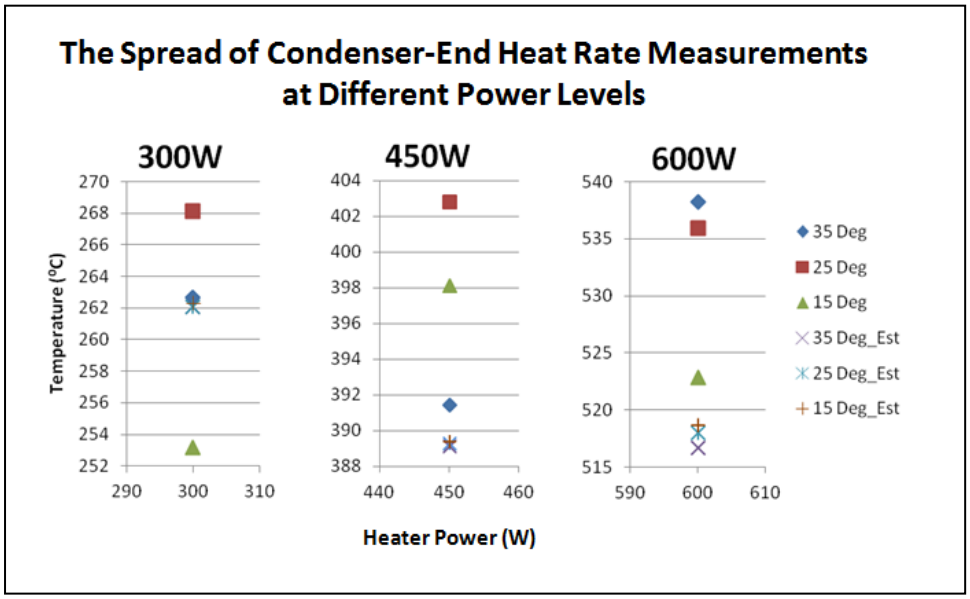

Figure 6.2: The spread of the condenser-end heat rate measurements for a range of power levels applied to the heater.

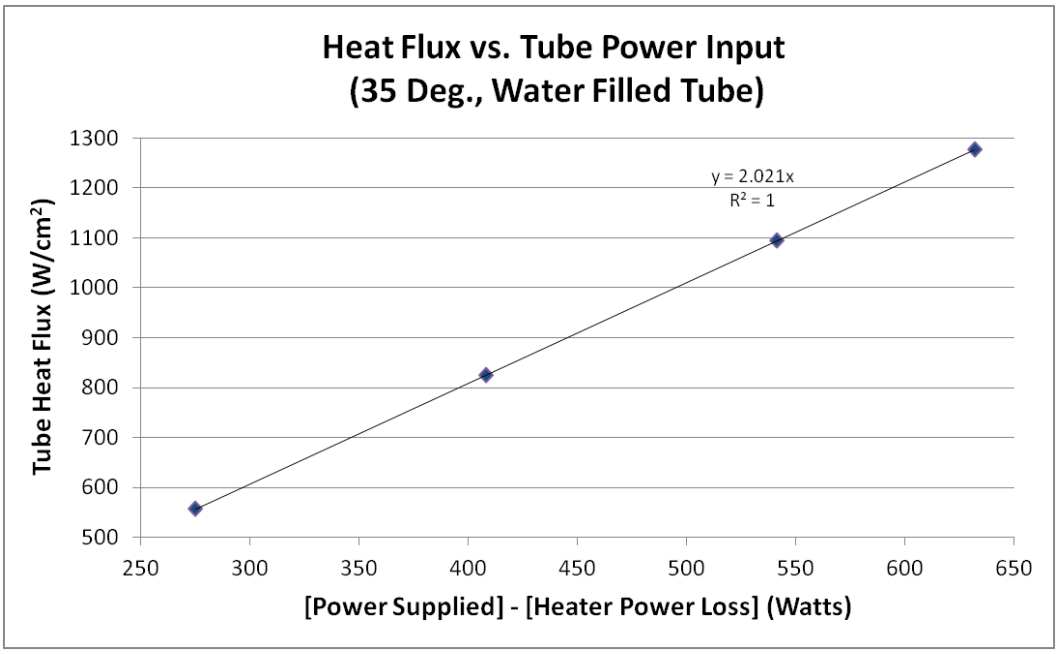

Figure 6.3: Total heat flux carried by the water-filled tube from the evaporator section (35 degree tilt).

6.2 Grooved IAS-Filled Thermosyphon

An attempt was also made to test the IAS-filled, helically grooved tube that had been tested as a part of the joint ASI/UAHuntsville study in [1]. However, this tube showed signs of defect in the early stages of testing. First, the thermistors spaced along the length of the tube showed an abnormal delay in the temperature rise at sequential locations in the adiabatic section during the transient startup. That is, the thermistor nearest to the heater would record a rise in temperature, followed by a rise in temperature at the next axial location up to fifteen minutes later, and so on. That time lag deviated substantially from normal operation, where the sequential temperature rise occurred within a few minutes or less. Additionally, when the tube had (supposedly) reached steady state operation, the measured calorimeter (condenser-end) heat rates were far lower than what had been observed for the water-filled tube, in addition to the results that had been reported for the same tube in [1]. The tube also demonstrated abnormally high operating temperatures, which seemed to indicate that the majority of the heat was dispersed through the adiabatic section, instead of by the fins. The heater values were fairly consistent with what was observed for the water-filled tube. The measurements for the calorimeter heat

rate are plotted in Figure 6.4. The exact cause of the defect could not be investigated due to the time limitations imposed on the study. However, it may be possible that the defect was caused by a pin hole leak or by the formation of non-condensable gases within the tube.

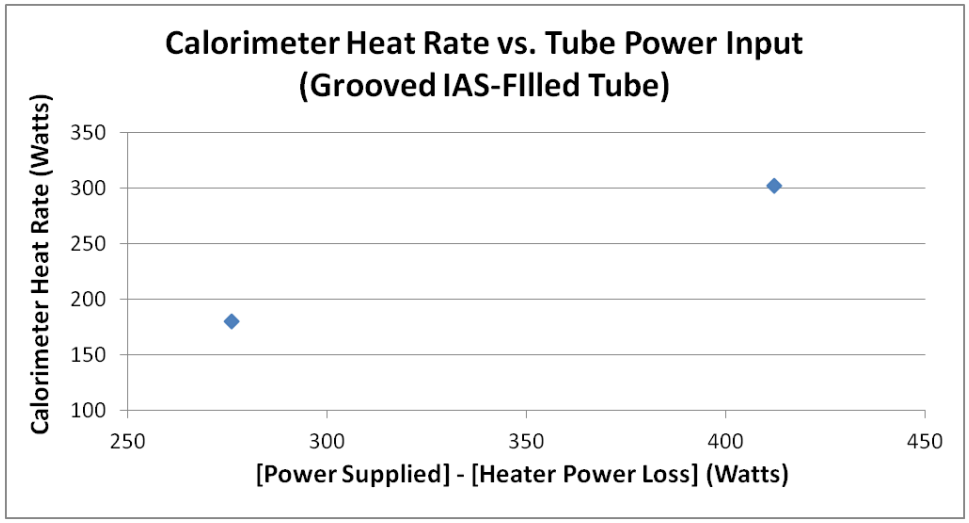

Figure 6.4: The measured calorimeter heat rate for the grooved water-filled tube.

6.3 Smooth-Walled, IAS-Filled Thermosyphon

Because the grooved IAS-filled thermosyphon was defective, a similar smooth-walled IAS thermosyphon was tested that had been used in prior UAHuntsville studies. The tube showed signs of burnout for a heater input of 600W. At this power level, approximately two hours was allowed for the tube to reach steady state operation. When data measurements were being taken, the heater temperature rose and the tube temperature dropped substantially, indicating a dry-out condition in the evaporator section. Once power applied to the heater was reduced, the tube operated normally. The heat rates measured using the calorimeter and the power loss curve are plotted in Figure 6.5 for heat input values up to 450 W. Since both methods of measurements demonstrated such good agreement during the water tube test, and because the estimated uncertainty associated with the heater power loss curve was shown to be small, the calorimeter measurements were only taken at the 35 degree tilt angle.

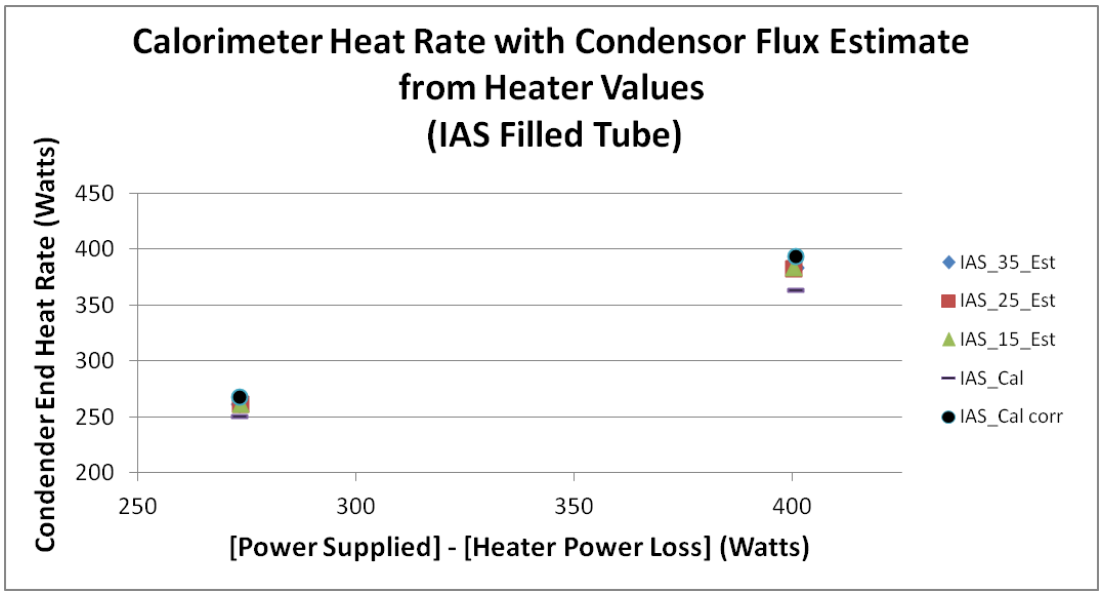

Figure 6.5: The condenser end heat rate for the IAS-filled tube measured using the calorimeter heat rate and the power-loss curve for the heater.

Upon first examining the data, the calorimeter measurements appeared to be a bit lower than the condenser-end heat rates derived using the power loss curve. With further inspection, it was noticed that the velocity readings for the IAS-filled tube were approximately 0.2 m/s lower on average than those measured while testing the water tube. This may have been an indication that there was a small air leak in the calorimeter. Those values were "corrected" using the velocity measurements that were taken while testing the water tube ("35 Deg_Cal_Corr" in Figure 6.5). As shown in the figure, data measured using both the calorimeter and the power loss curve were in good agreement.

6.4 Thermosyphon Performance Comparison

The condenser-end heat rates for the water and IAS-filled tubes are plotted together in Figure 6.6 for data taken at a 35 degree angular tilt. The data correspond to the heat rates measured using the power loss curve. Overall, the performance was nearly identical between the two tubes up to a heater input of 450 W. The trendline slopes and y-intercepts are very close. The results indicate that the internal grooves of the water-filled thermosyphon did not substantially increase the heat rate carrying capacity

over the smooth walled, IAS-filled tube at lower power levels. However, it is possible that the grooves played a role in extending the dryout limitation of the water-filled tube above a heater input of 450 W.

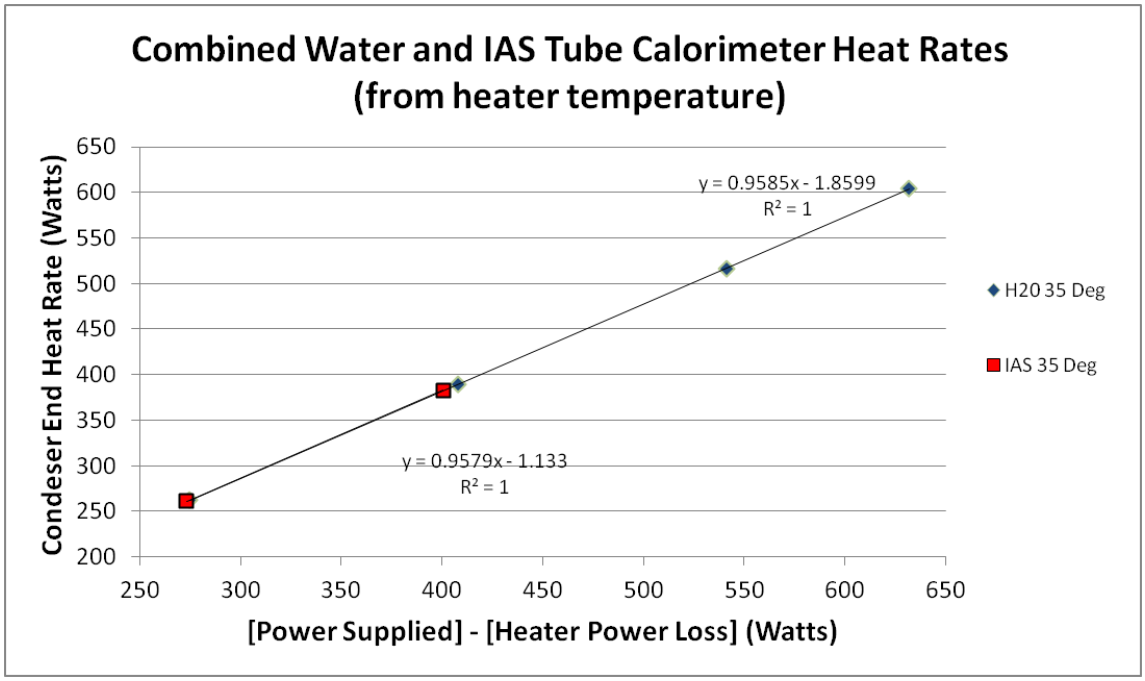

Figure 6.6: A performance comparison between the water and IAS-filled thermosyphons.

6.5 Theoretical Performance

The performance of both tubes was compared to the theoretical performance estimates generated by a range of thermosyphon limiting equations. Those equations are fully detailed in Chapter One. They were implemented using the overall dimensions of the thermosyphons tested in this study. The tube dimensions used in the calculations are shown in Table 6.1. A liquid volume of 15 mL was assumed, which is the amount of liquid used to charge the water-filled tube that was tested in this study. The theoretical performance was calculated for operating temperature spanning from 5 – 200 ^{o}C at intervals of 5 ^{o}C. The properties of water at the respective operating temperatures were generated using the NIST REFROP thermodynamic and transport property program.

Table 6.1: Thermosyphon dimensions that were used as input values for the thermosyphon limiting equations.

Variable	Value	Description
D (m)	7.94E-03	Diameter
A (m2)	4.948E-05	Cross Sectional Area
g (m/sec2)	9.81	Gravitational Constant
Le (m)	0.1778	Length of the Evaporator
Lc (m)	0.9144	Length of the Condenser
La (m)	2.1082	Length of the Adiabatic Section
L_tot (m)	3.048	Total Length of the Thermosyphon
d (m)	1.803E-04	Groove Depth
w (m)	2.794E-04	Groove Width

Figure 6.7 shows the predictions made by the limiting equations as well as the performance measured for the water and IAS-filled thermosyphons in this study. As detailed in the figure, the limiting equations cover a range of limiting modes including flooding, dryout, and boiling. In addition, the correlation given by Tien and Chung provides the entrainment limitation for thermosyphons with grooved wicks. The heat flux values for the water and IAS-filled tubes were calculated using the total heat carried by the tube from the heater ($Q_{tube} = Q_{in} - Q_{lost}$). As shown, the operational values obtained in this study fall well below the operational limit predicted by the broad range of limiting equations. Table 6.2 shows the axial heat flux values for the water and IAS tubes.

Table 6.2: The axial heat flux values for the water and IAS-filled tubes in W/cm^2.

Heater Input (Watts)	Axial Heat Flux, Water Filled Tube	Axial Heat Flux, IAS-Filled Tube
300	555.57	552.44
450	824.85	809.52
600	1093.75	
700	1276.54	

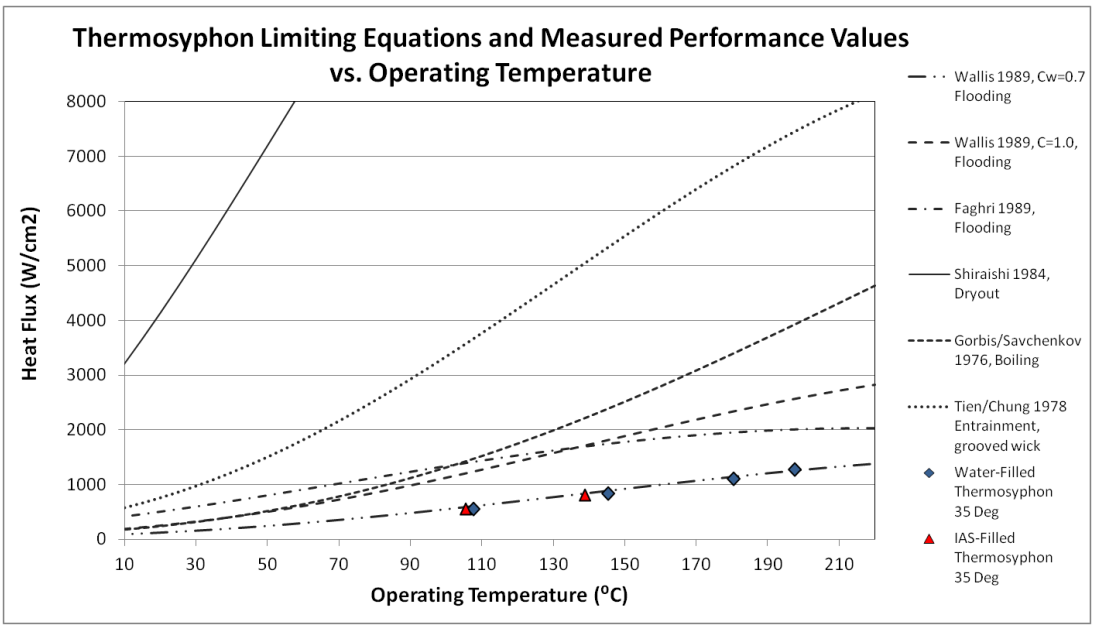

Figure 6.7: Performance measurement of the water and IAS-filled thermosyphons plotted against performance estimates from thermosyphon limiting equations.

CHAPTER SEVEN

CONCLUSION AND RECOMMENDATIONS

The performance of the water and IAS-filled tube were similar for heater input values up to 450 Watts. The results varied slightly from results found by ASI and UAHuntsville, which showed that the water tube outperformed the IAS-filled tube by approximately 9%. As noted earlier, the IAS-filled tube that was tested by ASI showed signs of a defect in this study. It is possible that the defect in the IAS-filled tube had just started to be reflected by a corresponding drop in performance when it was tested by ASI. Time constraints did not permit a thorough investigation of the source of the defect, however, it is surmised that the drop in tube performance may have been caused by a pin-hole leak or the formation of non condensable gases.

A maximum heat flux of 1,276.5 W/cm^2 was attained using the water-charged thermosyphon. This exceeds the heat flux rate attained by Rao in previous UAHuntsville studies, which was approximately 1043 W/cm^2. It's likely that the internal grooves of the water thermosyphon were the reason for attaining the high operational heat flux value. The performance predictions from thermosyphon limiting equations would also support this theory, as the equation corresponding to a grooved thermosyphon predicts a maximum heat transport capability that is greater than what is predicted by other contemporary equations that do not account for internal grooves. Correspondingly, the grooves in the water-filled tube may have prevented the evaporator dry-out at higher heater input values in comparison to the smooth walled IAS-filled tube. However, this is hard to completely verify by a closed form analysis since the liquid volume of the IAS-filled thermosyphon was not determined as a part of the study.

In general, the thermosyphon limiting equations over predicted the performance of the tubes at each of the heater input levels. One conclusion that can be drawn is that limiting equations are less than conservative, at least for the thermosyphon design tested in this study. A parametric analysis may be

beneficial in the future to determine the amount of variation caused by each of the particular variables in the respective equations. In addition, some investigative research may be warranted to consider the derivations of each of the applied limiting equations as well as the supporting empirical data. It's possible that the long, small diameter thermosyphon designs that were tested fell outside the typical range of application for the considered equations. One obvious exception is the correlation developed by Wallis (Cw = 0.7), which best predicted the heat flux of the thermosyphons tested in this study. Although the water thermosyphon never achieved a dry-out condition in the evaporator, the Wallis equation gave a nearly pin-point accurate prediction of the dryout conditions in the IAS-filled tube. The thermosyphons also showed no change in performance with angular tilt. This observation is appropriately accounted for in each of the limiting equations considered in this study, as none of them account for angular variation in their prediction of limiting heat rates.

Although the air calorimeter proved to be the less accurate method of measuring the condenser-end heat rate of the tubes, some improvements could be made to the current set-up to increase its reliability. First, a grid of thermistors could be used downstream of the fins to measure air temperature. This would provide a more accurate average and provide a better estimate of the bulk temperature. Also, a more leak proof calorimeter would have improved the results taken for the IAS-filled tube. This could be achieved by using rubber couplings in addition to increased amounts of duct tape at the joints.

Overall, it is evident that the IAS-filled tube (formerly called a "Qu-tube" when it was tested in [22]), offers no distinct performance advantage over the state-of-the-art in water thermosyphon technology for a 10 ft. long, 5/16 in. diameter tube. However, this observation does not invalidate high performance characteristics observed while testing the fluid at UCLA, as those studies focused specifically on the performance of the fluid in a copper biporous wick. Also, although there was no clear performance advantage in this study, IAS may still hold a distinct advantage over water in some circumstances, especially considering its potential compatibility with aluminum and aluminum alloys [1], [9]. In this case, the performance per unit weight provided by the IAS working fluid would be far greater than water. This is because aluminum is much lighter than copper and other metals that are commonly

used in conjunction with water in heat pipes and thermosyphons. This was shown by theoretically comparing the performance of equivalent copper and aluminum-water heat pipes in [1].

APPENDIX

Inorganic Aqueous Solution MSDS

Posnett International Co. Ltd.
679 Brea Canyon Road
Walnut, CA 91789-3078
Innovative Thermal Solutions
http://www.posnett.biz

Effective Date: July 14, 2009

24-hr Emergency Telephone for chemical emergency, spill, leak, exposure or accident:
CHEMTREC: 800-424-9300
International: 1-703-527-3887

MSDS – Material Safety Data Sheet

Inorganic Aqueous Solution (IAS) Heat Pipe Medium

1. Product Identification

Synonyms: Inorganic Aqueous Solution Heat Pipe Medium
Product Codes: 2.5

This product is a thin-walled tubing welded at both ends, which meets the definition of "article" per US OSHA 29 CFR 1910.1200 (c). However, an MSDS was prepared for possible handling of leaks or pipe ruptures.

2. Composition

The heat pipe contains an approximately 1.5% aqueous solution of the chemicals listed below. None of the chemicals is present in an amount of 1% or more of the solution. The exact concentration is proprietary.

Ingredient	CAS No	Hazardous
Sodium Peroxide	1313-60-6	Yes
Beryllium Oxide	1304-56-9	Yes
Titanium Diboride	12045-63-5	Yes
Cobaltic Oxide	1308-04-9	Yes
Boron Oxide	1303-86-2	Yes
Strontium Chromate	7789-06-2	Yes
Calcium Dichromate	14307-33-6	Yes
Magnesium Dichromate	14104-85-9	Yes
Potassium Dichromate	7778-50-9	Yes
Sodium Dichromate	10588-01-9	Yes
Silver Dichromate	7784-02-3	Yes

Page 1 of 8

3. Hazards Identification

The following information is in the event when the medium is exposed to air due to rupture of the housing materials.

Emergency Overview

DANGER! MAY CAUSE ALLERGIC REACTION. CANCER HAZARD. CAN CAUSE CANCER. Risk of cancer depends on duration and level of exposure.

Health Rating: 3 - Severe (Cancer Causing)
Flammability Rating: 0 - None
Reactivity Rating: 0 - None
Contact Rating: 3 - Severe (Corrosive)
Lab Protective Equip: GOGGLES & SHIELD; LAB COAT & APRON; VENT HOOD; PROPER GLOVES
Storage Color Code: White (Corrosive)

Potential Health Effects

Inhalation:
This substance is slightly toxic to internal organs if inhaled.
Ingestion:
Swallowing can cause burns of the mouth, throat, and stomach, leading to death.
Skin Contact:
None to minor irritation.
Eye Contact:
None to minor irritation.
Chronic Exposure:
Repeated or prolonged exposure can cause ulceration and perforation of the nasal septum, respiratory irritation, liver and kidney damage and ulceration of the skin. Ulcerations at first may be painless, but may penetrate to the bone producing "chrome holes." Known to be a human carcinogen.
Aggravation of Pre-existing Conditions:
Persons with pre-existing skin disorders, asthma, allergies or known sensitization to chromic acid or chromates may be more susceptible to the effects of this material.

---

4. First Aid Measures

The following information is in the event when the medium is exposed to air due to rupture of the housing materials.

Inhalation:
Remove to fresh air. If not breathing, give artificial respiration. If breathing is difficult, give oxygen. Get medical attention immediately.
Ingestion:
Give large quantities of water. Get medical attention immediately.
Skin Contact:
Immediately flush skin with plenty of water for at least 3 minutes while removing contaminated clothing and shoes. Wash clothing before reuse. Thoroughly clean shoes before reuse.
Eye Contact:
Immediately flush eyes with plenty of water for at least 3 minutes, lifting lower and upper eyelids occasionally. Get medical attention immediately.

---

5. Fire Fighting Measures

Fire:
Not combustible.
Explosion:
Not explosive.
Fire Extinguishing Media:
None
Special Information:
In the event of a fire, wear full protective clothing and NIOSH-approved self-contained breathing apparatus with full face piece operated in the pressure demand or other positive pressure mode.

---

6. Accidental Release Measures

Wear appropriate personal protective equipment as specified in Section 8. Spills: Sweep up and containerize for reclamation or disposal. Vacuuming or wet sweeping may be used.

---

7. Handling and Storage

Protect against physical damage. Remove and dispose of any spilled dichromates; do not return to original containers. Wash hands, face, forearms and neck when exiting restricted areas. Shower, dispose of outer clothing, change to clean garments at the end of the day. Avoid cross-contamination of street clothes. Wash hands before eating and do not eat, drink, or smoke in

workplace. Containers of this material may be hazardous when empty since they retain product residues (dust, solids); observe all warnings and precautions listed for the product.

---

8. Personal Protection

OSHA Permissible Exposure Limits (PEL; TWA=8-hr weighted average, C = ceiling)
Beryllium oxide: TWA = 0.002 mg/m^3 (as Be); C = 0.005 mg/m^3 (as Be)
Boron oxide: TWA = 15 mg/m^3
All chormates: C = 0.1 mg/m^3 (as CrO_3)
Sodium peroxide, titanium diboride, cobaltic oxide: none issued.

Ventilation System:
A system of local and/or general exhaust is recommended to keep employee exposures below the Airborne Exposure Limits. Local exhaust ventilation is generally preferred because it can control the emissions of the contaminant at its source, preventing dispersion of it into the general work area.
Skin Protection:
Wear impervious protective clothing, including gloves, lab coat, apron or coveralls, as appropriate, to prevent skin contact.
Eye Protection:
Use chemical safety goggles and/or full face shield where dusting or splashing of solutions is possible. Maintain eye wash fountain and quick-drench facilities in work area.

---

9. Physical and Chemical Properties

Appearance:
Dark brown liquid
Odor:
Odorless.
% Volatiles by volume @ 21°C (70°F):
0
Boiling Point:
100°C (212°F)
Vapor Density (Air=1):
No information found.
Vapor Pressure (mm Hg):
No information found.
Evaporation Rate (BuAc=1):

No information found.

---

10. Stability and Reactivity

Stability:
Stable under ordinary conditions of use and storage.
Hazardous Decomposition Products:
Burning may produce chrome oxides.
Hazardous Polymerization:
Will not occur.
Incompatibilities:
None.
Conditions to Avoid:
None.

---

11. Toxicological Information

-------\Cancer Lists\----------

Ingredient	---NTP Carcinogen--- Known	Anticipated	IARC Category
Strontium Chromate (7789-06-2)	Yes	No	1
Calcium Dichromate (14307-33-6)	Yes	No	1
Magnesium Dichromate (14104-85-9)	Yes	No	1
Potassium Dichromate (7778-50-9)	Yes	No	1
Sodium Dichromate (10588-01-9)	Yes	No	1
Silver Dichromate (7784-02-3)	Yes	No	1

---

12. Ecological Information

Environmental Fate:
When released into the soil, this material may leach into groundwater. When released into water, this material is not expected to evaporate significantly. This material may bioaccumulate to some

extent. When released into the air, this material may be removed from the atmosphere to a moderate extent by wet deposition.
Environmental Toxicity:
No information found.

---

13. Disposal Considerations

Whatever cannot be saved for recovery or recycling should be handled as hazardous waste and sent to a RCRA approved waste facility. Processing, use or contamination of this product may change the waste management options. State and local disposal regulations may differ from federal disposal regulations. Dispose of container and unused contents in accordance with federal, state and local requirements.

---

14. Transport Information

Domestic (Land, D.O.T.)

Proper Shipping Name: Oxidizing liquid, toxic, N.O.S., (Contains potassium dichromate and sodium dichromate)
Hazard Class: 6.1/5.1
UN/NA: UN3099
Packing Group: II

International (Water, I.M.O.)

Proper Shipping Name: Oxidizing liquid, toxic, N.O.S., (Contains potassium dichromate and sodium dichromate)
Hazard Class: 6.1/5.1
UN/NA: UN3099
Packing Group: II

---

15. Regulatory Information

The following information also apply for Strontium Dichromate (7789-06-2), Calcium Dichromate (14307-33-6), Magnesium Dichromate (14104-85-9), Sodium Dichromate (10588-01-9), and Silver Dichromate (7784-02-3).

--------\Chemical Inventory Status - Part 1\---------------------------------

Ingredient	TSCA	EC	Japan	Australia
Potassium Dichromate (7778-50-9)	Yes	Yes	Yes	Yes

--------\Chemical Inventory Status - Part 2\---------------------------------

		--Canada--		
Ingredient	Korea	DSL	NDSL	Phil.
Potassium Dichromate (7778-50-9)	Yes	Yes	No	Yes

--------\Federal, State & International Regulations - Part 1\----------------

	-SARA 302-		------SARA 313------	
Ingredient	RQ	TPQ	List	Chemical Catg.
Potassium Dichromate (7778-50-9)	No	No	No	Chromium com

--------\Federal, State & International Regulations - Part 2\----------------

		-RCRA-	-TSCA-
Ingredient	CERCLA	261.33	8(d)
Potassium Dichromate (7778-50-9)	10	No	No

Chemical Weapons Convention: No TSCA 12(b): Yes CDTA: Yes
SARA 311/312: Acute: Yes Chronic: Yes Fire: No Pressure: No Reactivity: No

PROP 65 WARNING:
THIS PRODUCT CONTAINS A CHEMICAL(S) KNOWN TO THE STATE OF CALIFORNIA TO CAUSE CANCER.

Australian Hazchem Code: 1WE
Poison Schedule: S6

WHMIS:
This MSDS has been prepared according to the hazard criteria of the Controlled Products Regulations (CPR) and the MSDS contains all of the information required by the CPR.

---

16. Other Information

NFPA Ratings: Health: **3** Flammability: **0** Reactivity: **0**

Posnett International Co. Ltd.
679 Brea Canyon Road
Walnut, CA 91789-3078
Innovative Thermal Solutions
http://www.posnett.biz

REFERENCES

1. S. Cooke, “Qu Tubes for High Temperature Heat Rejection Phase I, Final Report,” Anal. Services, Inc., Huntsville, AL, Tech. Rep. ASI-STONE-10-20, Dec. 31, 2010.

2. *Flow, Level, and Environmental Handbook and Encyclopedia,* 8th Ed. Omega Eng., Inc., 2009.

3. A. Faghri, “Two-phase closed thermosyphons,” in *Heat Pipe Science and Technology*, New York, NY: Taylor and Francis, 1995, ch.6, pp. 341-434.

4. J. B. Blackmon and S. F. Entrekin, “Preliminary Results of an Experimental Investigation of the Qu Superconducting Heat Pipe,” Univ. of Alabama in Huntsville, Huntsville, AL, Grant NCC 8-200, 2008.

5. I. Catton, “Studies of IAS for Phase Change Heat Transfer Applications,” presented at the Thermal Management Technologies Conf., Point Clear, AL, 2011.

6. *ASHRAE Handbook. Fundamentals*, American Society of Heating, Refrigerating, and Air-Conditioning Engineers, Inc., Atlanta, GA, 1993.

7. A. F. Mills, “Natural convection,” in *Basic Heat and Mass Transfer*, 2nd ed., Upper Saddle River, NJ: Prentice Hall, 1999, ch. 4, sec. 4.4, pp. 293-301.

8. T. Robinson, private communication, 2010.

9. I. Catton and S. W. Reilly, “Utilization of Advanced Working Fluids With Biporous Evaporators,” *J. of Thermal Sci. and Eng. Applicat.*, Vol. 3, June, 2011.

10. R. Reid, private communication, Los Alamos National Laboratory, Feb. 15, 2010.

11. M. C. H. McKubre and F. L. Tanzella, “Thermal Property Analysis of the Qu Supertube, Part I: Thermal Conduction Studies,” SRI International, July 1999, unpublished.

12. F. L. Tanzella and M. C. H. McKubre, “Thermal Property Analysis of the Qu Supertube, Part II: Mass Flow Calorimetry,” SRI International, Aug. 1999, unpublished.

13. Q. Leland *et. al.*, “Investigation of Super Tube Structure and Performance (Postprint),” AFRL, Wright-Patterson AFB, OH, Rep. AFRL-RZ-WP-TP-2011-2078, Apr. 2010.

14. D. S. Alexander, “Advanced Energetics for Aeronautical Applications,” NASA Langley Research Center, Hampton, VA, Rep. CR-2003-212169, Feb. 2003.

15. S. F. Entrekin, “Experimental Investigation of the Qu Tube Heat Pipe,” M.S. thesis, Dept. Mech. and Aerospace Eng., Univ. of Alabama in Huntsville, Huntsville, AL, 2008.

16. P. R., Rao, “Thermal Characterization Tests of the Qu Tube Heat Pipe,” M.S. thesis, Dept. Mech. and Aerospace Eng., Univ. of Alabama in Huntsville, Huntsville, AL, 2009.

17. B. E. Hurless and F. H. Froes, “Lowering the Cost of Titanium,” *The AMPTIAC Quarterly*, Vol. 6, No.2.

18. Q. Yuzhi, “Superconducting Heat Transfer Medium,” U.S. Patent 6 132 823, Oct. 17, 2000.

19. Q. Yuzhi, “Medium Having a High Heat Transfer Rate,” U.S. Patent 6 811 720, Nov. 2, 2004.

20. Q. Yuzhi, “Method for Producing a Heat Transfer Medium and Device,” U.S. Patent 6 911 231, Jun. 28, 2005.

21. Q. Yuzhi, “Superconducting Heat Transfer Medium,” U.S. Patent 6 916 430, Jul. 12, 2005.

22. R. O. Cummings *et. al.*, “Thermal Characterization of Superconducting Solid State Heat Pipes,” in *TFAWS 2006*, College Park, MD, Aug., 2006.

23. SRI International Final Reports. Available: http://www.q-t-g.com/testing.html

24. Atmospheric Pressure at Huntsville International Airport, United States – KHSV. Available: http://timetric.com/index/atmospheric-pressure-khsv-metar/

25. G. Wallis, *One-Dimensional Two-Phase Flow*, McGraw-Hill, New York, 1969.

26. A. Faghri, M. M. Chen and M. Morgan, “Heat Transfer in Two-Phase Closed Conventional and Concentric Annular Thermosyphons,” *ASME J. Heat Mass Transfer*, Vol. 111, pp. 611-618, 1989.

27. M. Shiraishi, M. Yoneya and A. Yabe, “Visual Study of Operating Limit in the Two-Phase Closed Thermosyphon,” *Proc. 5th Int. Heat Pipe Conf*., Tsukuba, Japan, pp. 11-17, 1984.

28. Z. R. Gorbis and G. A. Savchenkov, “Low Temperature Two-Phase Closed Thermosyphon Investigation,” *Proc. 2nd Int. Heat Pipe Conf.*, Bologna, Italy, pp. 37-45, 1976.

29. C. L. Tien, “A Simple Analytical Model for Counter-Current Flow Limiting Phenomena with Vapor Condensation,” *Letter in Heat and Mass Transfer*, Vol. 4, pp. 231-238, 1977.

30. C. L. Tien and K. S. Chung, “Entrainment Limits in Heat Pipes,” *Proc. 3rd Int. Heat Pipe Conf.*, Palo Alto, California, pp. 36-40, 1978.

31. Thermal conductivity plots. Available: http://www.engineeringtoolbox.com